



Michigan Technological University
Create the Future Digital Commons @ Michigan Tech

Dissertations, Master's Theses and Master's
Reports - Open

Dissertations, Master's Theses and Master's
Reports

2015

DEVELOPMENT OF A CELL MORPHOLOGICAL ANALYSIS TOOL TO EVALUATE THE ULTRASOUND VIBRATIONAL EFFECTS ON CELL ADHESION

Joseph M. Smith
Michigan Technological University

Follow this and additional works at: <https://digitalcommons.mtu.edu/etds>



Part of the [Biomedical Engineering and Bioengineering Commons](#), and the [Electrical and Computer Engineering Commons](#)

Copyright 2015 Joseph M. Smith

Recommended Citation

Smith, Joseph M., "DEVELOPMENT OF A CELL MORPHOLOGICAL ANALYSIS TOOL TO EVALUATE THE ULTRASOUND VIBRATIONAL EFFECTS ON CELL ADHESION", Master's Thesis, Michigan Technological University, 2015.

<https://doi.org/10.37099/mtu.dc.etds/974>

Follow this and additional works at: <https://digitalcommons.mtu.edu/etds>



Part of the [Biomedical Engineering and Bioengineering Commons](#), and the [Electrical and Computer Engineering Commons](#)

DEVELOPMENT OF A CELL MORPHOLOGICAL ANALYSIS TOOL TO
EVALUATE THE ULTRASOUND VIBRATIONAL EFFECTS ON CELL ADHESION

By

Joseph M. Smith

A THESIS

Submitted in partial fulfillment of the requirements for the degree of

MASTER OF SCIENCE

In Biomedical Engineering

MICHIGAN TECHNOLOGICAL UNIVERSITY

2015

© 2015 Joseph Smith

This thesis has been approved in partial fulfillment of the requirements for the Degree of
MASTER OF SCIENCE in Biomedical Engineering.

Department of Biomedical Engineering

Thesis Advisor: *Keat G. Ong*

Committee Member: *Rupak Rajachar*

Committee Member: *Glen E. Archer*

Department Chair: *Sean J. Kirkpatrick*

Table of Contents

Abstract.....	vii
1. Introduction.....	1
<i>1.1 Fibrotic Body Response and Current Deterrents</i>	<i>1</i>
<i>1.1.1 Foreign Body Response</i>	<i>1</i>
<i>1.1.2 Current Anti-Fouling Techniques</i>	<i>3</i>
<i>1.2 Implantable Devices.....</i>	<i>5</i>
<i>1.2.1 Bone-Anchored Prostheses</i>	<i>5</i>
<i>1.2.2 Sensors</i>	<i>6</i>
<i>1.3 Mechanotransduction and Application of Ultrasound.....</i>	<i>7</i>
<i>1.3.1 Mechanotransduction of Fibroblast Cells</i>	<i>8</i>
<i>1.3.2 Application of Ultrasound.....</i>	<i>9</i>
<i>1.4 Project Objectives</i>	<i>12</i>
2. Ultrasound Driver Circuit.....	14
<i>2.1 Regulator Circuit</i>	<i>14</i>
<i>2.2 Function Generator Circuit</i>	<i>15</i>
<i>2.3 Amplifier Circuit</i>	<i>16</i>
<i>2.4 Piezoelectric Transducer</i>	<i>17</i>
<i>2.5 MSP430FG4618 Microcontroller.....</i>	<i>18</i>
<i>2.6 Transducer Characterization.....</i>	<i>19</i>
3. MATLAB Image Processing	23
<i>3.1 Uploading an Image</i>	<i>23</i>
<i>3.2 Image Management.....</i>	<i>24</i>
<i>3.3 Image Processing Functions.....</i>	<i>24</i>
<i>3.3.1 Gray Image</i>	<i>25</i>
<i>3.3.2 Background Removal</i>	<i>26</i>
<i>3.3.3 Black and White Image</i>	<i>28</i>
<i>3.3.4 Removing Border</i>	<i>29</i>
<i>3.3.5 Smoothing Image</i>	<i>30</i>
<i>3.3.6 Locating the Peaks</i>	<i>32</i>

3.4 <i>Image Analysis Functions</i>	33
3.4.1 <i>Cell Count</i>	33
3.4.2 <i>Cell Density Plot</i>	36
3.4.3 <i>Cell Area</i>	38
3.4.4 <i>Cell Roundness</i>	40
3.4.5 <i>Filter</i>	42
4. Experiments	43
4.1 <i>Materials</i>	43
4.3 <i>Ultrasound Procedure</i>	44
4.4 <i>Staining Procedure</i>	45
4.5 <i>MATLAB Analysis</i>	45
4.5.1 <i>Cell Viability</i>	45
4.5.2 <i>Cell Density</i>	45
4.5.3 <i>Cell Morphology</i>	46
4.6 <i>Statistical Analysis</i>	46
5. Results and Discussion	47
5.1 <i>Cell Viability</i>	47
5.2 <i>Cell Density</i>	50
5.3 <i>Cell Morphology</i>	54
5.3.1 <i>Cell Roundness</i>	54
5.3.2 <i>Cell Area</i>	57
5.4 <i>Effectiveness of the Ultrasonic Vibrations</i>	59
5.5 <i>Ultrasound Model for Treatment</i>	60
5.5.1 <i>Mechanical Effects</i>	62
5.5.2 <i>Thermal Effects</i>	63
5.5.3 <i>Ultrasound Treatment Model</i>	64
6. Conclusion	66
6.1 <i>Future Work</i>	67
References	68

Abstract

Fibroblast encapsulation is a stage of the wound healing process in which the implanted device is separated from the biological environment due to the formation of fibrotic tissue. Uncontrolled adhesion of fibroblasts, called fibrosis, has the ability to inhibit an implanted device's functionality over its lifetime. Over time, fibroblasts have been shown to cause loosening and failure of bone-anchor implants which could include the possibility of harming the patient. The encapsulating process could also hinder the sensitivity of implanted biosensors operating in the body for continuous monitoring. Unfortunately, the antifouling surfaces which are commonly used on implanted devices to control the fibrotic response are not able to maintain their efficiency over an extended period of time and have a possibility to disrupt the device's functionality. This project presents the development of a cell morphology analysis tool and an *in vitro* ultrasound system to investigate the effect of ultrasound on cell adhesion with the possibility of leading to further work in the control of fibroblast adhesion and prolonging the function and life of the implanted devices.

1. Introduction

A major setback with implanted devices is the occurrence of uncontrolled fibroblast adhesion [1, 2]. Fibrosis can impede the function of the device and potentially harm the patient. Devices implanted into the body for an extended period of time will experience the fibrotic response. Many of the current techniques utilize an anti-fouling coating on the device, but the protective coating has a short lifespan in which the fibrotic response will eventually overcome [1]. Mechanical forces had been shown to alter the behavior of cells within the body and affect the adhesion properties of fibroblast cells [2]. This project focuses on the development of an *in vitro* ultrasound application system and a cell morphology analysis tool, and application of these systems to investigate the effect of mechanical forces on cell behavior, which will lead to better control of the fibrous response to the implanted material.

1.1 Fibrotic Body Response and Current Deterrents

The foreign body response is a part of the wound healing process and is responsible for the protection of the biological environment from foreign implanted objects. The initiation of the foreign body response after a material is implanted into the body is tasked to remove or phagocyte the material. Implanted materials have routinely used an anti-fouling coating for protection from the response in order to lengthen their lifespan.

1.1.1 Foreign Body Response

The Foreign Body Response is activated when an object is implanted into the body [1, 3]. The extent of the response is related to the total damage received by the biological system due to the injury, the type of material and its interaction with the blood, the amount of cell necrosis, and the initial tissue response [1, 3]. Most implants are exposed to blood due to the blood vessels within the connective tissue and that results in the activation of the thrombotic response [3]. The ability of the proteins to adhere to the

surface of the material directly affects the activation of the inflammatory process and controls many cellular response [1, 3].

The main types of activated cells operating in the implant site are determined by the inflammatory process timeframe [1, 3]. Neutrophils primarily operate in the acute inflammation period which transpires in the initial stage after the injury and results in phagocytosing of microorganisms and foreign materials [3]. Sensors, such as glucose sensors which rely on the interstitial fluid for sensing the blood glucose levels, are not able to operate correctly during the acute inflammation period due to the increase in bioactivity in the area [4, 5]. Chronic inflammation occurs after the acute inflammation period and experiences the increased presence of monocytes, lymphocytes, and most importantly macrophages, which produces a high volume of biological active products. Macrophages release growth factors to initiate cell migration, differentiation, and tissue remodeling within the implant site. The macrophages guide the process of angiogenesis and the growth of connective tissue as the repair continues to the injury site with the formation of granulation tissue. The granulation tissue begins with an increased amount of proteoglycans, but fibrotic capsulation process results in the excess synthesis of collagen [1-3, 5].

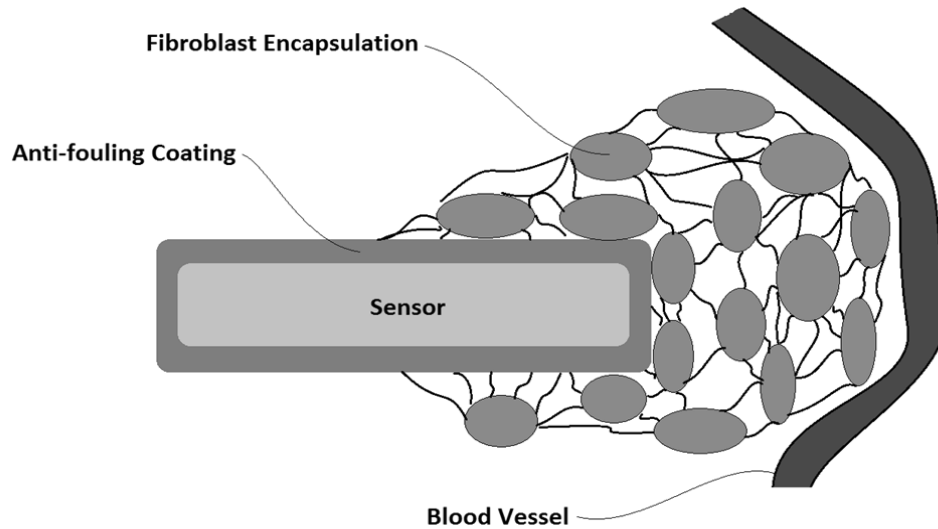


Figure 1.1 – Fibroblast encapsulation of an implanted sensor blocking the sensor’s access to the biological environment causing the sensor to lose functionality.

The encapsulation process of the Foreign Body Response consists of foreign body giant cells and granulation tissue shielding the implanted material from the biological environment as shown in Figure 1.1. The cell thickness of the capsule is determined by the surface to volume ratio of the foreign material [1]. Smooth surfaces will experience a lower level of cell adhesion and collagen growth compared to a rough surface. Prolonged presence of macrophages on the surface of the implant can lead to the excess buildup of extracellular components such as fibronectin, proteoglycans, hyaluronic acid, and interstitial collagen [1-3]. Encapsulation of the implanted material ensures the biological environment is restricted, but unfortunately many devices, such as sensors, rely on the access to the environment in order to function.

1.1.2 Current Anti-Fouling Techniques

Cellular adhesion and encapsulation of an implanted device can cause failures within the mechanical system. Failure could include lead detachment, electrical shorts, breakdown of the membrane, and bio-fouling [6]. The physiochemical properties of the implanted material affect the fibrotic response and can be used to control the fibrotic

response post-implantation. The shape, size, surface chemicals, morphology and porosity can vary the macrophage adhesion rate. However, there is no surface manipulation to be developed to prevent the fibrous encapsulation process [1, 2]. Developments to reduce the response involve coating the surface of the device to mask the underlying material and reduce the protein absorption and cell interaction. Polyethylene glycol and heparin based coatings are two methods to diminish the fibrotic response on the materials [1].



Figure 1.2 – Surface of an implant (black) coated with hydrophilic polyethylene glycol chains (gray) used for anti-fouling. The polyethylene glycol chains attract water molecules which form a barrier between the biological system and the surface of the implant [7].

Polyethylene glycol is a common method to halt the adhesion of extracellular matrix proteins to the surface of implanted materials in order to reduce the biological response. The ability to resist the adsorption of proteins is a result of the polyethylene glycol's hydrophilic characteristic. The polyethylene glycol chains extend perpendicular from the material's surface and create anti-fouling properties through steric repulsion and chain compression as shown in Figure 1.2. The hydrophilic characteristic of polyethylene glycol chains create a water buffer to separate the surface of the implant and the proteins within the biological environment [7]. The anti-fouling capabilities of

polyethylene glycol are determined by the molecular weight, grafting density, and polymer chain architecture [8].

The addition of an anti-fouling coating could decrease the severity of the biological response to the implanted material, but the coating could also inhibit the sensing capabilities of the implanted sensors [5]. The ability to adhere the coating to the device can prove troublesome, and the coating has to be able to withstand the implantation procedure. Also, the coating could inhibit access to the sensing enzyme or component, disrupting the sensor's capabilities [6].

1.2 Implantable Devices

Devices implanted into the body are affected differently by the foreign body response, but in many cases can hinder the device's function and cause problems for the patient. Uncontrolled fibrosis can cause the formation of irregular skin folds along the mounting fixtures of mechanical prosthetics and allow for infections to develop. Implantable sensors rely on their access to the biological environment, but the adhesion of fibroblast on the surface restricts their access. A reduction of fibroblast adhesion to the surface of implants, such as bone-anchored prostheses or implantable sensors, can extend the lifespan and reliability of the devices.

1.2.1 Bone-Anchored Prostheses

In 2005, it was recorded in the United States that 1.6 million people were living with a loss of a limb, and the number has been projected to increase to 3.6 million by year 2050 [9]. Most cases of amputees were due to trauma (~45%) or cardiovascular issues with the presence of diabetes mellitus (~38%) [9]. The increasing rate of diabetes affecting the population has increased the demand of amputations [9]. In 2009, \$8.3 billion in hospital costs were associated with amputations [9].

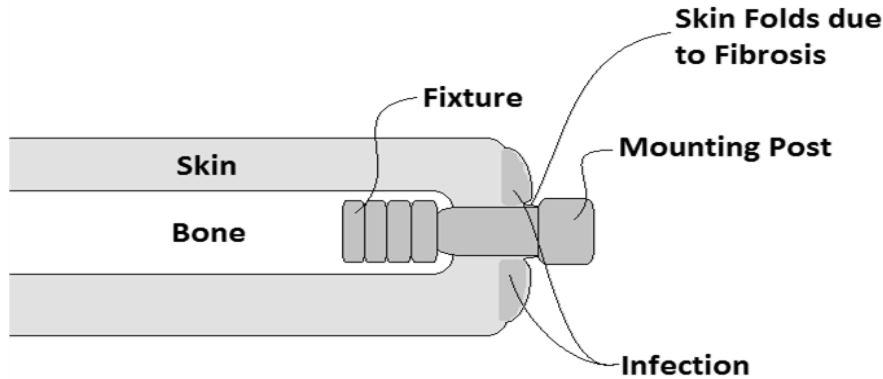


Figure 1.3 – Bone-anchored prosthesis with skin folds caused by the fibrotic process. The skin folds could allow microbes into the tissue and cause infections within the area.

Bone-anchoring prostheses utilize a mounting rod surgically inserted into the patient's bone at the amputation site. The mounting rod provides a fixation point for the prostheses by extending through the skin and fat tissue of the amputated limb [2]. The fibrosis process during the use of bone-anchor prostheses was caused by abnormal cell growth around the mounting post and led to irregular skin folds around the implant. The skin folds along the mounting rod can present stability problems with the device, as well as region with an increase in risk of infections. These variables count lead to the eventual failure of the prosthetic device [2]. Enhanced fibrosis activity at the surface of implanted device raises concerns for the long-term success of many biomedical implants and is a major deterrent for many prosthetic options. As the quality of life for amputees has increased, a call for devices with a longer lifespan has expanded. [2].

1.2.2 Sensors

Implantable sensors allow for continuous monitoring of the patient and rely heavily on the device's ability to provide information accurately. The sensors can experience a reduction in their capabilities over their lifespan due to fibrosis' ability of restricting access to the biological environment. For example, implantable miniaturized glucose sensors are being developed for the monitoring of glycemia of diabetic patients

[4, 5]. The device will reduce the possibility of long term complications of diabetes and hopefully improve the quality of life of the patient. When the device is exposed to fibrosis, the response of the implantable sensor undergoes a significant decrease due to the reduction in the accessibility to the vascular system as shown in Figure 1.1. Many implantable sensors rely on the ability to be in contact with blood circulation, and fibrous encapsulation has been shown to slow the diffusion rate of glucose to the sensor [5, 6, 10]. In order to use the device long term, the fibrosis process needs to be controlled so a consistent reading is acquired.

According to the American Diabetes Association, in 2012, 29.1 million people in the United States were recorded to have a form of diabetes, and the number is projected to increase to 59 million by the year 2050 [11, 12]. According to the American Diabetes Association, patients with Type-1 diabetes should self-monitor their blood glucose levels 3 to 4 times a day, while patients with Type-2 diabetes should test at least once daily. The only method to currently test the patient's glucose level is through the "finger prick" technique which is inconvenient and causes discomfort [13]. An implanted glucose monitor can lessen or eliminate the necessity of the "finger prick" and allow for continuous monitoring of the blood glucose. Unfortunately, studies have shown that the implanted sensors were not able to maintain reliable monitoring due to drift in the sensor's current [10]. The fibrous capsule can decrease the diffusion rate of molecules and proteins to the sensor and increase the delay in the sensor's response. Through testing it was shown that the foreign body capsule could not adequately provide oxygen and glucose to the sensor due to the avascular capsule, thus increasing the delay in the sensor's response [4, 10].

1.3 Mechanotransduction and Application of Ultrasound

Mechanical forces have been shown to have the ability to control cell behavior, specifically cellular adhesion through methods utilizing vibrational platforms which were in direct contact with the cells [2]. Ultrasound provides an in-vitro method to produce similar forces utilizing compressive waves upon the cells without an invasive treatment.

1.3.1 Mechanotransduction of Fibroblast Cells

Mechanotransduction is the ability of the cell to convert a mechanical stimulus into a chemical signal. The mechanical forces are transmitted through the cell's adhesion molecules, tight junctions, and surface receptors. The receptors receive and transmit the mechanical properties of the external environment to the cell interior through the use of communication between the integrin and actin-cytoskeleton as shown in Figure 1.4 [14]. The cells utilize the information it receives from the external environment to adjust their behavior and ensure their optimal placement within the environment.

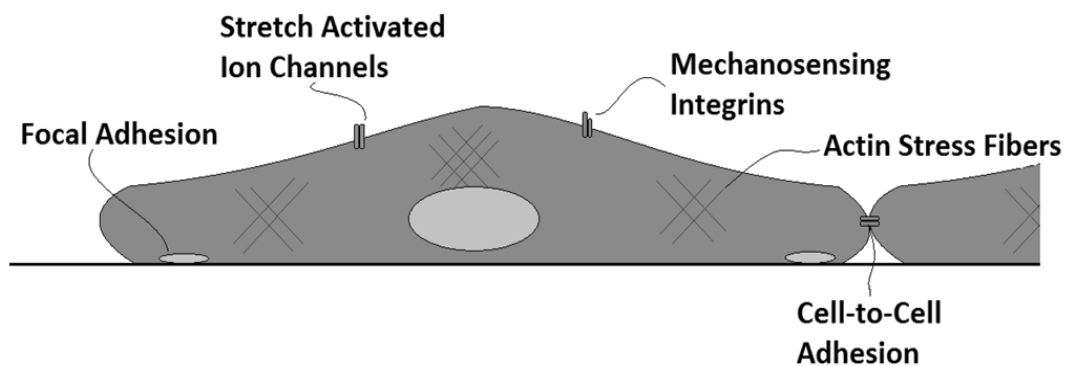


Figure 1.4 – Mechanotransduction of fibroblast cells. The cell's mechanosensing integrins and stretch activated ion channels send information about the external environment to the nucleus through the use of the actin cytoskeleton. Then, the nucleus issues a response by controlling the cell-to-cell and focal adhesions.

A mechanical loading platform has been fabricated with magnetoelastic materials to test fibroblast adhesion on a cyclic vibrating surface with the use of an AC magnetic field. The vibrating surface was spin coated with polyurethane and chitosan layers in order to facilitate cell adhesion and viability. The vibration frequency was set to 170 – 176 kHz with approximate 0.15 μm displacement amplitude. The vibrated cells had no variation in cell viability compared to the control which signifies that no cell apoptosis

was caused by the vibrations. The cells on the vibrated test showed a considerable increase in the cell detachment suggesting that the cell's adhesion properties were affected by the vibrations [2].

Other studies have shown that biaxial cyclic strains on fibroblasts led to the activation of a distinct group of genes. The activation of the fibronectin and nidogen-2 genes while the cells were experiencing a mechanical strain displayed the role of mechanical forces in affecting the cell's adhesion properties. The cyclic strain leads to a rapid gene response which was only transient and disappeared completely after 6 hours [14]. A similar transient gene response would allow for a short duration treatment while also not having a lasting effect on the cells after the treatment has been concluded.

1.3.2 Application of Ultrasound

Ultrasound utilizes a piezoelectric material's ability to convert electrical energy into acoustic energy. The acoustic energy transmits through media in the form of compressive waves. The frequency of an ultrasound device is above 20 kHz with therapeutic devices ranging from 0.75 to 3 MHz. The frequency of the device, along with the output intensity, determines the penetration depth of the compressive wave.

$$\text{Equation 1.1} \quad \delta = \frac{2c_0^3\alpha}{\omega^2} \quad [15]$$

Equation 1.1 displays the calculation to determine the penetration depth of the ultrasound with losses attributed to the attenuation coefficient (α). The acoustic diffusivity (δ) is dependent heavily on the frequency (ω) to determine the losses within the tissue. A 1 MHz signal has the penetration depth of approximately 3 to 5 cm in depth while a 3 MHz signal can penetrate 1 to 2 cm in depth. The density of the medium also affects the depth of the ultrasonic waves. Tissues with higher water content reduce the amount of absorption compared to tissues abundant in protein [16].

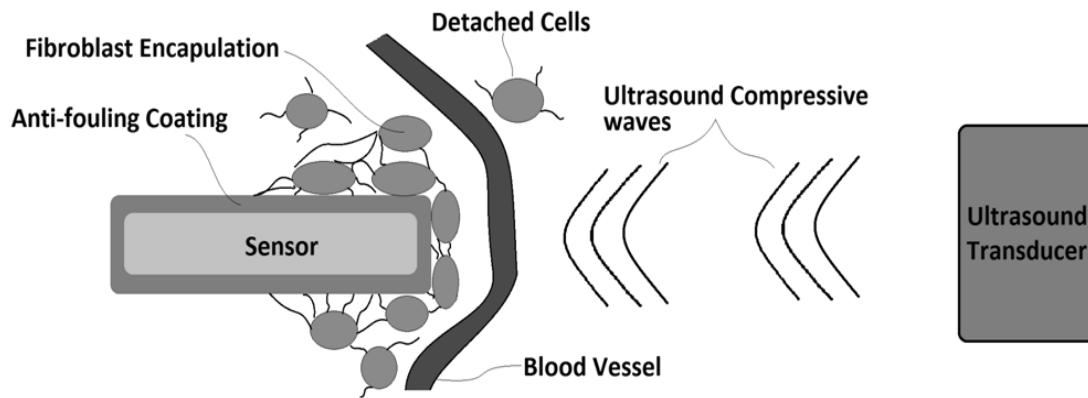


Figure 1.5 – Ultrasound used to control the fibroblast adhesion on the implanted sensor. The fibroblast cells detach and allow the sensor more access to the biological environment.

Mechanical vibrations have been shown to affect cell adhesion with the use of magnetoelastic materials. Unfortunately, magnetoelastic materials were required to be in direct contact with cells in order to provide the mechanical forces as shown in Figure 1.6. The ultrasound's compressive waves were able to replace the implantable vibrating source while providing similar mechanical effects to control cellular adhesion as shown in Figure 1.5. The benefit of ultrasound treatment was that there were no additional modifications required of the implanted device which could inhibit its intended function. Another difference was the mechanical forces acting on the cells were not in a uniform direction as was with the magnetoelastic materials. The ultrasound's compressive waves contacted the cells in multiple directions depending on the cell and transducer locations. In the ultrasound study, the cells only receive mechanical forces in the longitudinal direction as seen in Figure 1.6.

The main difference of mechanical force applied during the uniaxial direction and the compressive forces of the ultrasound is that the magnetoelastic uniaxial forces acted on the focal adhesion points of the cell. The stimulus acting directly on the points of adhesion could have ultimately affected the adhesion strength of the cell which would not be a factor during the ultrasound treatment.

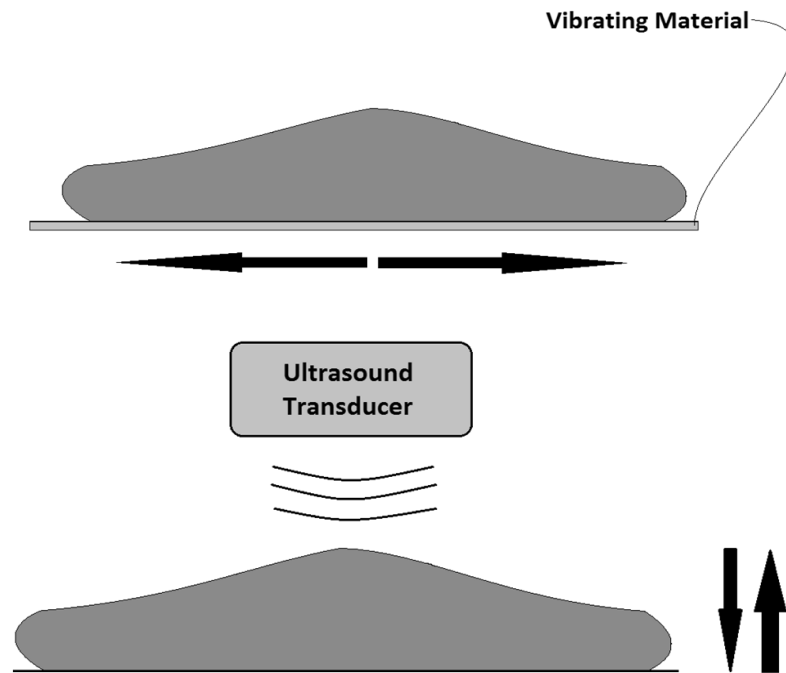


Figure 1.6 – Previous testing results showed that fibroblast adhesion was controllable through the use of mechanical vibrations in the latitudinal direction (top), but during the ultrasound treatment, the vibrations could also occur in the longitudinal direction (bottom).

Ultrasound does have adverse effects, such as heating and cavitations within the biological system, and measures to ensure safety of the patient throughout the treatment are required [17]. Common techniques to lower the heating effect of the ultrasound include lowering the amplitude of the acoustic wave if possible or by pulsating the output wave utilizing a certain duty cycle. Pulsation of the output is the most frequently used method to lessen the heating of tissue in ultrasound techniques in which the treatment is ongoing for an extended period of time [17-19]. Many soft tissue therapeutic ultrasound devices maintain an intensity output between 50 mW/cm^2 and 1 W/cm^2 for a 15 minute treatment [17] with varying duty cycles depending on the location and depth of the targeted area. For therapeutic treatments utilizing a continuous output, the intensity is required to be lowered to a range of 5 mW/cm^2 to 50 mW/cm^2 [19] in order to avoid heating issues.

1.4 Project Objectives

Prior research has shown that mechanical forces were able to disrupt the adhesion capabilities of fibroblast cells to a surface [2]. The goal of this research was to provide evidence of an ultrasound device's ability to control the cellular adhesion of fibroblast cells. It was required to display the relationship between the intensity of the ultrasound's compressive waves and the detachment of the cells while not showing signs of additional dead cells due to heating and cavitation effects within the vibrated area.

An ultrasound driving circuit was built to provide a stable electrical signal to the transducer with the user's ability to control the frequency and amplitude. The circuit was required to provide a stable output signal throughout each experiment which consisted of consecutive 1 hour trials with the total experiment length of 3 hours. A controllable output frequency had to be achieved through the use of a microcontroller with the frequency displayed on a LCD screen, and the output intensity must be able to be varied by the user in between each trial. The circuit is described in Chapter 2.

MATLAB® (2010a, TheMathWorks, Inc., Natick, Massachusetts, United States.) was used to process the cell images and provide consistent analysis of the data. The MATLAB software allowed for a more automated and customizable image processing tool compared to other programs such as the ImageJ [20] software. ImageJ is a commonly used program to process and analyze microscopic images of cells. Common imaging techniques utilize macros to automate the analyzing functions. A problem arises in the ImageJ software when more detailed analyzing techniques are required, such that the information needs to be transferred to another program, such as MATLAB, for data analysis. The use of MATLAB over the entire project would reduce the necessity of transferring the data and eliminate unnecessary steps to the cell analysis process. Each cell had to be counted and analyzed individually while extracting characteristics such as their area and roundness. The MATLAB software also has the ability to analyze the change in the density of cells throughout the entire cell plate image in order to examine the change in densities of the vibrated and non-vibrate sections. Chapter 3 provides a description of the MATLAB image processing software.

Analysis of the cell plates was done to determine the affect of the ultrasound on the cells. The vibrated and non-vibrated sections were examined by their cell density, viability, and morphology by utilizing the MATLAB software. The data was investigated with the use of SAS JMP to determine statistical significance, and presented in Chapter 4-5.

2. Ultrasound Driver Circuit

In order to successfully test the ultrasound effects on the fibroblast cells, an ultrasound driving circuit was designed to produce an oscillating output signal to the transducer. Precise control of the signal's amplitude and frequency was required in order to successfully characterize the ultrasound's effect on the fibroblast cells. The driver circuit utilized a stable power system to maintain the correct output intensity for the transducer throughout the longevity of each experiment. An AC-DC convertor and a DC-DC convertor were used to provide a 40 V external power supply to the ultrasound unit. The regulator and amplification circuits used the 40 V external supply to create a ± 20 V saturation limits for the amplification circuit. The peak output amplitude of 20 V provided an output intensity ranging from 3.2 μW to 7.9 μW which provided compressive waves of varying pressures.

2.1 Regulator Circuit

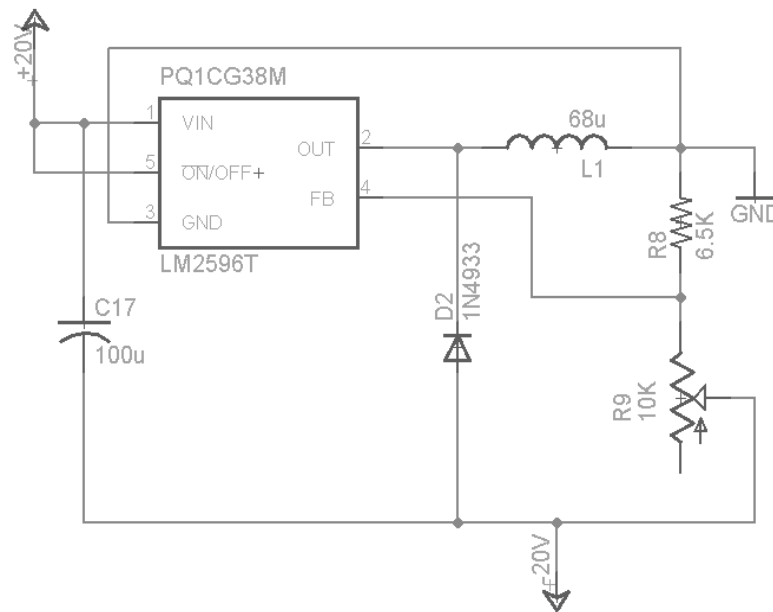


Figure 2.1 – The switching regulator circuit used to convert the power source of 0 V – +40 V to - 20 V – +20 V. The regulator utilized in the circuit was the PQ1CG38M step-down (Buck) switching regulator.

The 40 V DC signal was converted to +20 V – -20 V through the use of a switching regulator. The switching regulator converted the +40 V source to a +20 V source. The +20 V source was then used as a ground, creating power sources of +20 V, 0 V, and -20 V for the on-board components. PQ1CG38M step-down (Buck) switching regulator was selected for creating the +20 volt source as the ground signal in order to separate the +40 V supply into ± 20 V. The switching regulator was used to lower the power loss due to the voltage reduction of 20 V. A linear regulator converts the initial voltage to a lower voltage by dissipating the unwanted power through heat. A linear regulator is inefficient due to the high power losses in the voltage reduction process; therefore a switching regulator is used. A switching regulator utilizes an electrical switch and a controller to ensure the correct output voltage is acquired. Switching regulators are beneficial for their ability to expand the life of battery supplied devices due to their power efficiency.

The AD5932 and MSP430FG4618 microcontroller utilized a 3.3V power source, and the 50 MHz crystal oscillator required a 5 V source to create a clock signal for the function generator seen in Section 2.2. The 5V power source was produced through the use of a LM7805C 5 V linear voltage regulator utilizing the 20 V source. The 3.3 V source was produce through the use of an LD1117v33 linear regulator utilizing the 5 V source to lessen the voltage drop, thus reducing the dissipated power through heat.

2.2 Function Generator Circuit

The AD5932 function generator was used for its ability to precisely control the frequency of the output signal with the assistance of the MSP430 microcontroller. The FSYNC, SCLK, SDATA, and CTRL signals were supplied by the MSP430 microcontroller to control the output frequency, in reference to the AD5942 function generator manual. The function generator utilized a power source of 3.3 V and a 50 MHz external clock. The 50 MHz clock on the MCLK pin was used in the process of calculating the selected output frequency. An 800 mV output signal produced at the selected frequency had a DC bias of 400 mV. A high pass filter with a cutoff frequency of 10 Hz was required to remove the DC component of the signal and generated a pure

AC sine wave signal. If the DC component remained in the signal, the amplification circuit would enlarge the signal and would force the signal into saturation. The output signal of the function generator was connected to the amplification circuit.

2.3 Amplifier Circuit

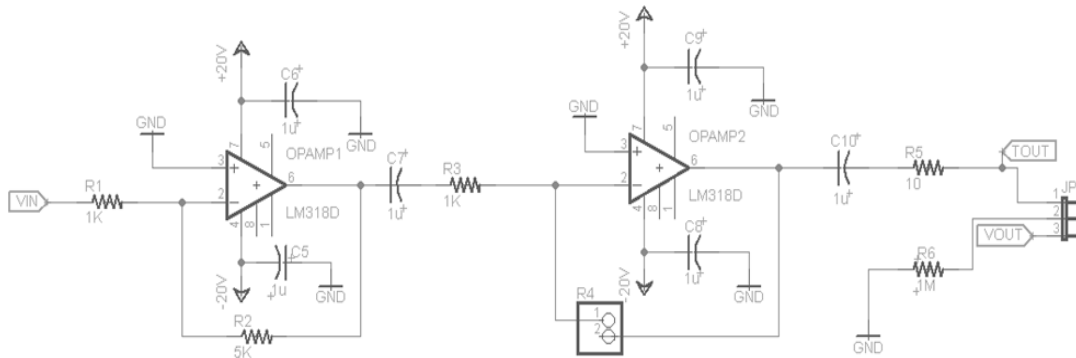


Figure 2.2 – The amplification circuit utilized a two stage inverting operation amplifier circuit. The first stage has a gain of 5 and the second stage was controlled by a potentiometer with a gain ranging from 1 to 20.

The amplification circuit was used to control the amplitude of the transducer signal. The input AC signal from the function generator had a peak-to-peak voltage of 800 mV. The amplification process involved utilizing a two stage inverting amplification circuit. The first stage of the amplification circuit had a gain of 5, while the second stage's gain was controlled through the use of a potentiometer with the gain ranging from 1 to 10. A coupling capacitor was placed in-between the first stage output and the input of the second stage for the reduction of the DC noise added during amplification. The output of the second stage in the amplification circuit provided a signal with amplitude ranging from 2 V to 20 V (4 V to 40 V peak-to-peak).

The operational amplifiers chosen for the amplification circuit were the LM318 general purpose amplifier due to their ability to fulfill the slew rate and saturation voltage requirements. The slew rate accounted for the rate of voltage change which can be achieved by the integrated chip. The LM318 has a slew rate of 50 V/μs, allowing for the 1 MHz output signal to obtain a signal with 40 V peak-to-peak amplitude without

encountering a slew rate limitation. Slew rate limitation of the signal would cause a disturbance in the frequency and the power output of the transducer.

2.4 Piezoelectric Transducer



Figure 2.3 – Ultrasound Transducer with a stainless steel housing and PVC handle

The ultrasound transducer utilized the electric signal from the ultrasound circuit and transformed it into acoustic signal through the use of a piezoelectric material. The piezoelectric material has the ability to expand and compress in the presence of an oscillating electrical signal. The oscillation of the piezoelectric material created an acoustic wave. The acoustic signal formed a compressive wave which entered the body and provided mechanical and thermal effects upon the biological system. The transducer directed the acoustic wave in the direction of the target area to ensure the treatment was provided to the correct location.

The piezoelectric transducer utilized a modified PZT-4 crystal with a resonance at 1 MHz and was 38 mm in diameter. The resonance impedance was less than $10\ \Omega$ and the static capacitance is $2600\ \text{pF} \pm 20\%$ at 1 kHz. The housing material was made of stainless steel, with a polyvinyl chloride (PVC) handle. The transducer was connected to the ultrasound circuit through the use of a BNC connector.

2.5MSP430FG4618 Microcontroller



Figure 2.4 - MSP430FG4618 experimenter board. The LCD screen shown displayed the output frequency of the ultrasound transducer.

The MSP430 microcontroller was a 16-bit, low power microcontroller which allowed for multiple input and output selections, as well as a LCD screen. The microcontroller was required to receive input from two push buttons in order to control the output frequency of the transducer. The MSP430's LCD screen displayed the output frequency of the device. The output pins on the microcontroller were used to control the AD5932 function generator by sending serial data commands. The system had the possibility of introducing errors into the frequency calculation if the selected frequency changed before the calculation was completed. A delay between the frequency selection and the output commands to the AD5932 was set to 2.5 seconds to eliminate the likelihood of producing an error.

The MSP430 sent commands to the AD5932 through the use of four pin parallel data transmissions to setup the output frequency. The pins used were the FSYNC, SCLK, SDATA, and CTRL. The FSYNC was the frame synchronization signal which

notifies the AD5932 data was being transmitted. The SCLK was the clock used during the data transmission. The frequency was set through the SDATA pins through the use of two 4 byte data transmissions, most significant byte (MSB) and least significant byte (LSB).

Equation 2.1

$$M = \frac{f_{out} * 2^n}{f_{MLK}}$$

In equation 2.1, the M value computed the information required to set the output frequency of the device. The value M was converted to binary and split into the eight bytes, four MSB and 4 LSB. Finally, the CTRL was set high to enable the output signal to the amplification circuit.

2.6 Transducer Characterization

In order to illustrate the ultrasonic vibrational intensity, calculations were done to determine the pressure of the ultrasonic waves, as well as resultant cell displacement in different mediums. The three vibrational intensities selected for the trials, -25 dBm, -22 dBm, and -21 dBm, were found experimentally through the use of a spectrum analyzer. The mediums selected were blood, liver, and fat, which would be encountered in the targeted areas for the treatment. The difference in the acoustic impedance of the mediums affected the intensity of the ultrasonic wave at its intended target. The acoustic impedances of blood and liver were known to be $1.66 \text{ kg} / (\text{m}^2\text{s}) \times 10^6$, and impedance of fat is $1.33 \text{ kg} / (\text{m}^2\text{s}) \times 10^6$.

Equation 2.2

$$P = \sqrt{2IZ}$$

Equation 2.3

$$Z_o = \frac{P}{Z\omega}$$

Table 2.1

The selected intensities are shown with their conversions from power (dBm) to pressure (Pa) and particle displacement (μm) within common mediums of the body for a 1 MHz signal.

Intensity (dBm)	Intensity (Watts)	Pressure (Pa) Blood/Liver	Displacement (μm) Blood/Liver	Pressure (Pa) Fat	Displacement (μm) Fat
-25	3.2E-06	3240.17929	0.001951915	2900.29	0.002436225
-22	6.3E-06	4576.874899	0.002757154	4096.76	0.003441259
-21	7.9E-06	5135.338099	0.003093577	4596.64	0.003861156

Pressure and particle displacement values were used to categorize the effect that the acoustic intensity has on the cells. The calculations were used to illustrate relationship between the ultrasonic intensities and cell densities, viability, and morphology to provide an accurate model for the ultrasound treatment.

The ultrasound intensity across the entire cell plate was not consistent due to the placement of the Aquaflex Ultrasound Gel Pad. The ultrasound gel pad facilitated the transmission of the ultrasound compressive waves through the plate and to the targeted cells. In order to calculate the intensity of the compressive wave at the location of the cells, a piezoelectric receiver was used in replacement of the cells, and the received signal was analyzed by a spectrum analyzer. The intensity of the signal was determined throughout the plate to show the correlation of the ultrasound intensity and the gel pad. The gel pad used was measured as 14 mm in diameter, and the cell plate was measured to be 35 mm in diameter. The plate was marked across its diameter in 2 mm intervals, and the gel pad was placed in the center of the plate. The intensity at each interval was recorded. Then the plate was rotated upon the gel pad, and the test was repeated to show consistency upon running multiple trials during the cell experiments. The intensity plots were utilized in the analysis of the cell density plots in order to determine the ultrasound's effect on the fibroblast cell adhesion.

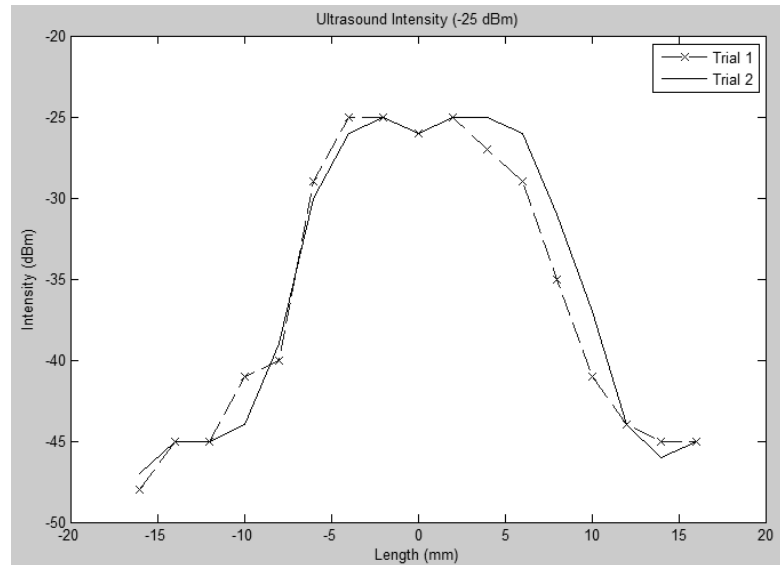


Figure 2.5 – The ultrasound intensity across the cell plate during the -25 dBm trials with the gel pad located at the approximately position -7 mm to 7 mm.

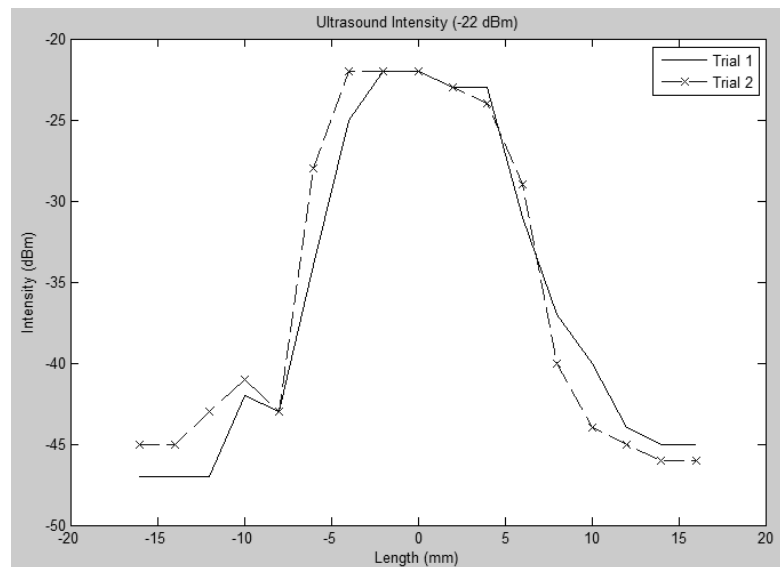


Figure 2.6 – The ultrasound intensity across the cell plate during the -22 dBm trials with the gel pad located at the approximately position -7 mm to 7 mm.

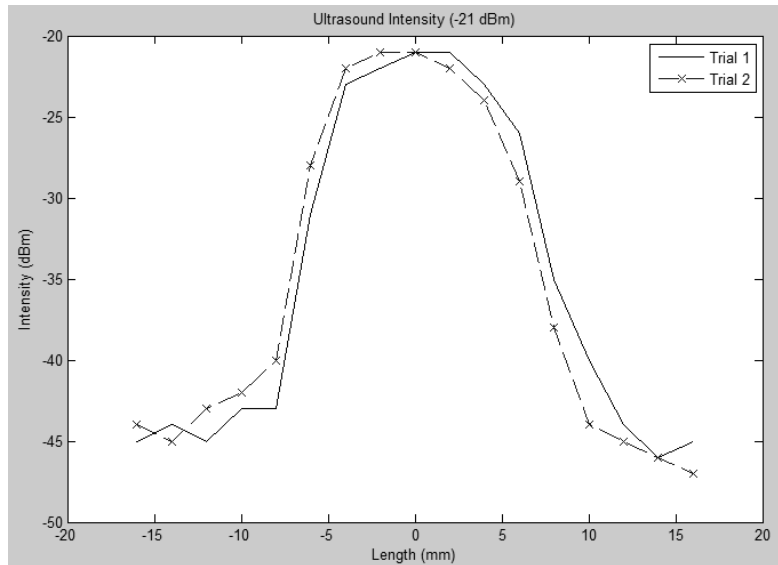


Figure 2.7 – The ultrasound intensity across the cell plate during the -21 dBm trials with the gel pad located at the approximately position -7 mm to 7 mm.

The intensity plots in Figures 2.5-2.7 demonstrated the steep increase in ultrasound intensity with the aid of the gel pad and displayed the effects of the gel pad assistance in the transmission of the ultrasonic waves. Outside of the gel pad, the ultrasound intensity was found to be approximately -45 dBm due to the ultrasound vibrations radiating throughout the entire cell plate. The variation in the peak intensity, for example at the -1 mm, 0 mm, and -1 mm positions in Figure 2.5, could be attributed to the differences in the gel thickness or the contact between the gel pad and cell plate. Variations in the width of the gel pad could be the origin of the discrepancies in the intensity plot widths.

3. MATLAB Image Processing

MATLAB was used to analyze the cells after the experiment was completed to test the effect of the ultrasound treatment. The software allowed for live-dead analysis, cell morphology analysis, and cell density analysis of each trial. A graphical user interface (GUI) was created to assist in the image processing.

3.1 *Uploading an Image*

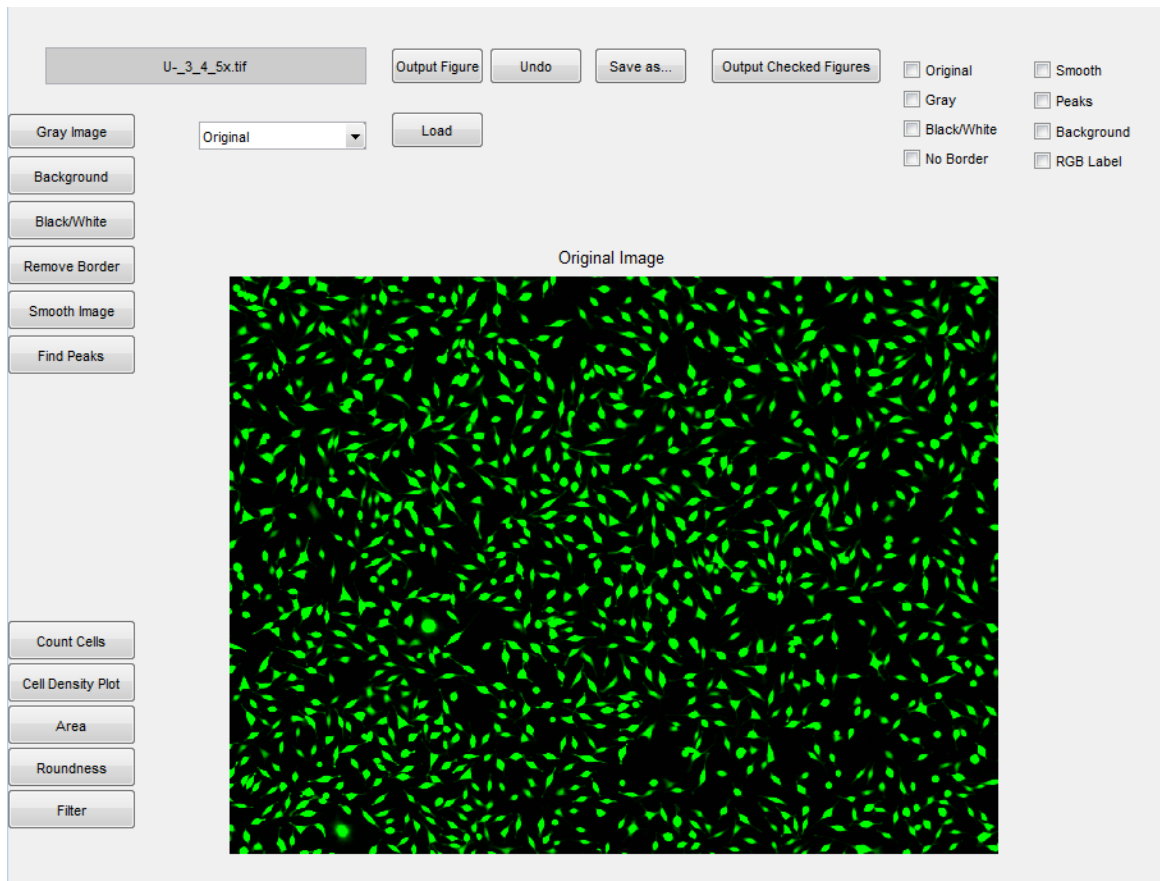


Figure 3.1 – ImageGUI was designed to process the images of each cell trial and analyze the individual cells. An image was uploaded into the GUI, and the image file is saved in the MATLAB workspace under the variable ‘Original’.

The GUI allowed for images to be uploaded into the program through the use of the ‘Image File’ text box. The image was placed in the same directory as the GUI

MATLAB file or the GUI MATLAB file was required to have a target to the image directory. The GUI provided the current image which had been uploaded into the program as shown in Figure 3.1

3.2 Image Management

Once the image was uploaded into the GUI, the image file was saved in the MATLAB workspace under the variable 'Original'. The GUI allowed the user to manipulate the image according to the user's requirements, and each process was saved in the workspace under unique variables. If repeated use of a similar process is required, such as repeated use of the 'Smooth' function on the same image, each previous image would be overwritten with the new image. To save the image as a new variable name, the 'Save as...' function saved the image variable to the workspace with the user assigned title. The saved variable in the workspace was used to further process the images outside the GUI. The 'Output Figure' button placed the current figure into a new popup window with a custom title. Another way to output images in new windows was to use the check boxes and 'Output Checked Figures' button. These features allowed the user to compare images during the image processing. An 'Undo' function permitted for the user to revert back to the previous process and reloads the previous image into the GUI.

3.3 Image Processing Functions

The ImageGUI allowed for the uploaded images to be processed by the users in a multiple ways. Each time the image was altered, it was saved in the MATLAB workspace under the corresponding variable name.

3.3.1 Gray Image

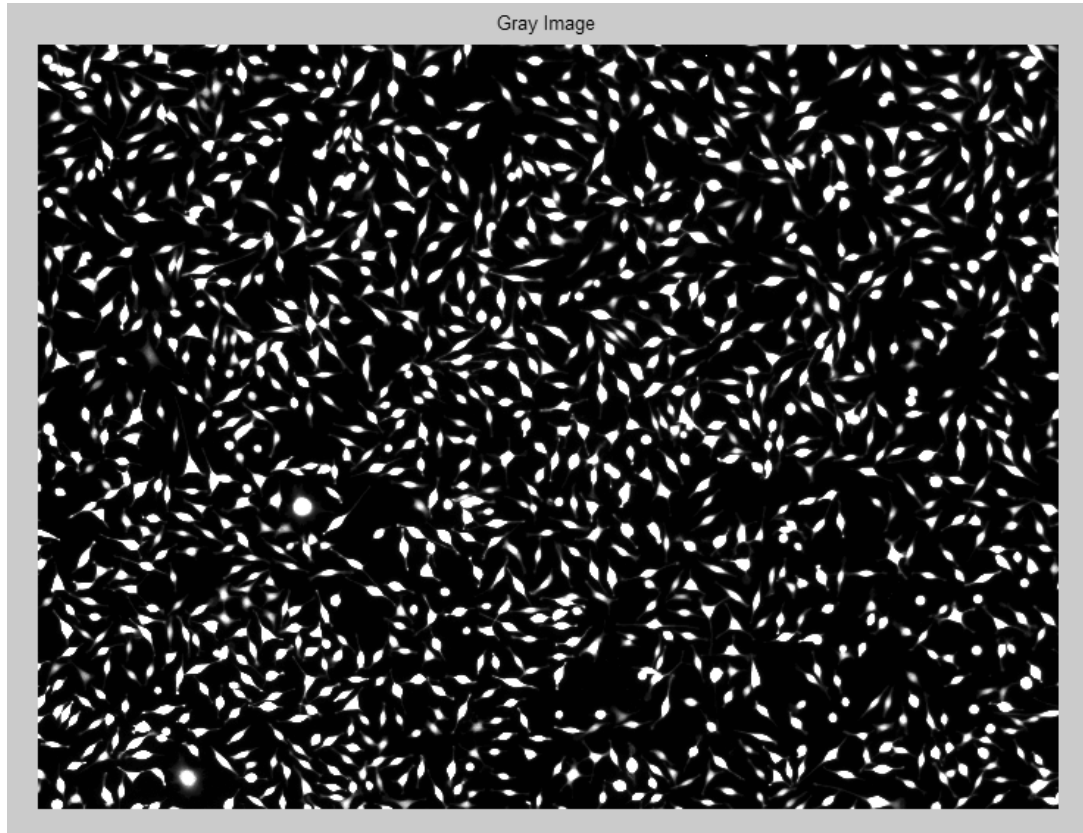


Figure 3.2 – The ‘Gray Image’ function converted all colors on the image into a gray and black image to lower the amount of data for each pixel.

The ‘Gray Image’ function converted the multicolored image into a gray and black. The function utilized the MATLAB code of *rgb2gray(RGB)*, with the variable ‘RBG’ to represent the colored image. The RGB image contains 24 bits of data per pixel while the gray image contains only 8 bits. The conversion from a colored image to a grayscale image would lessen the data amount of the image and enhance the speed of the processing and analyzing functions. The smaller data size image was able to be processed by the imaging functions at a faster rate than a multicolored image.

3.3.2 Background Removal

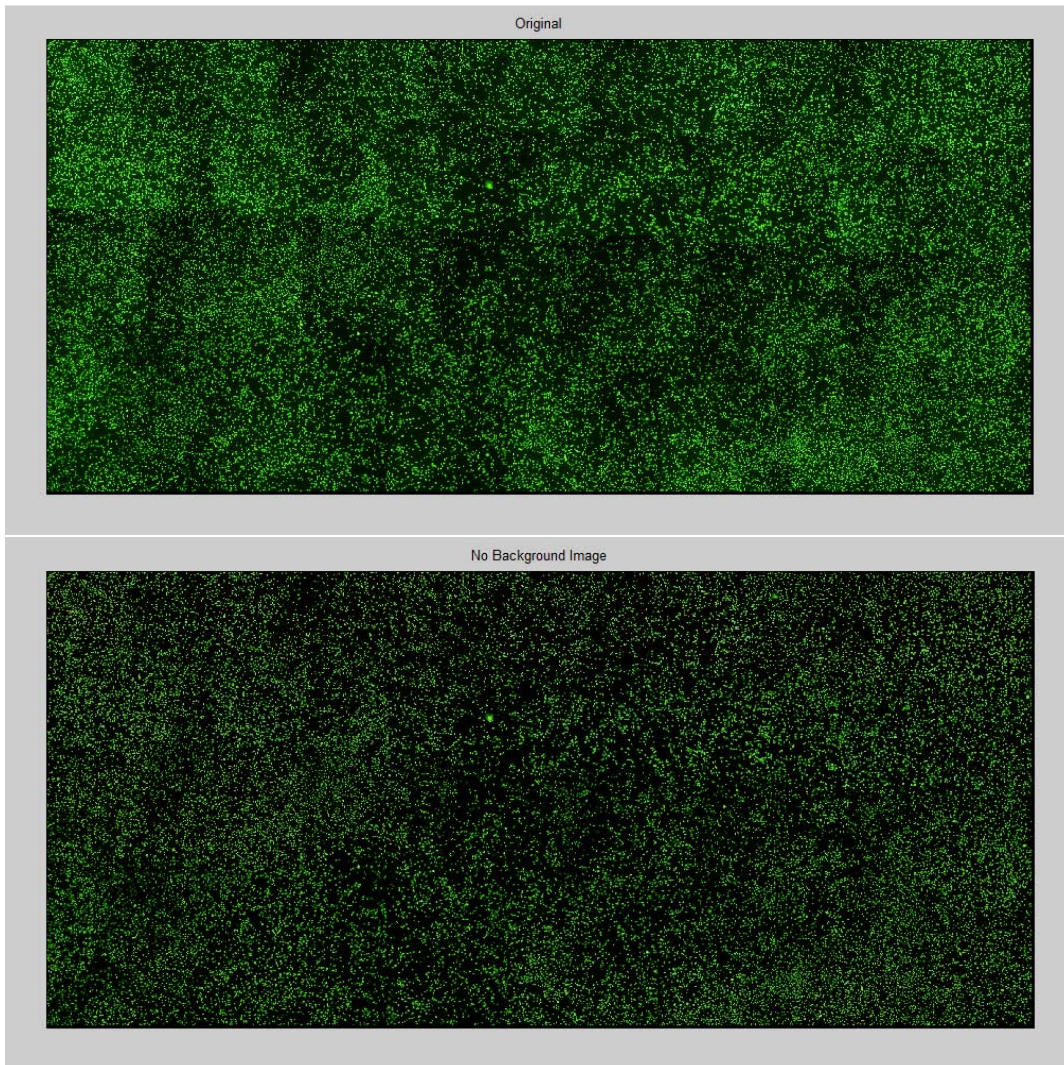


Figure 3.3 – (Top) Original image without processing shows a multi-contrast image due to the multiple images which were placed together. (Bottom) The image shown was after using the ‘Background’ function to remove the inconsistencies of contrast within the background.

Removing the background of the image through the use of the ‘Background’ function eliminated any inconsistency with the background shading. Some images had irregularities with the background contrast due to the intensity setting of the camera, and the ‘Background’ function corrected the issue. Also, the backgrounds of multiple images differed when they were assembled together as shown in Figure 3.2 (top), and when the

background was removed, the image became more uniform as seen in Figure 3.2 (bottom).

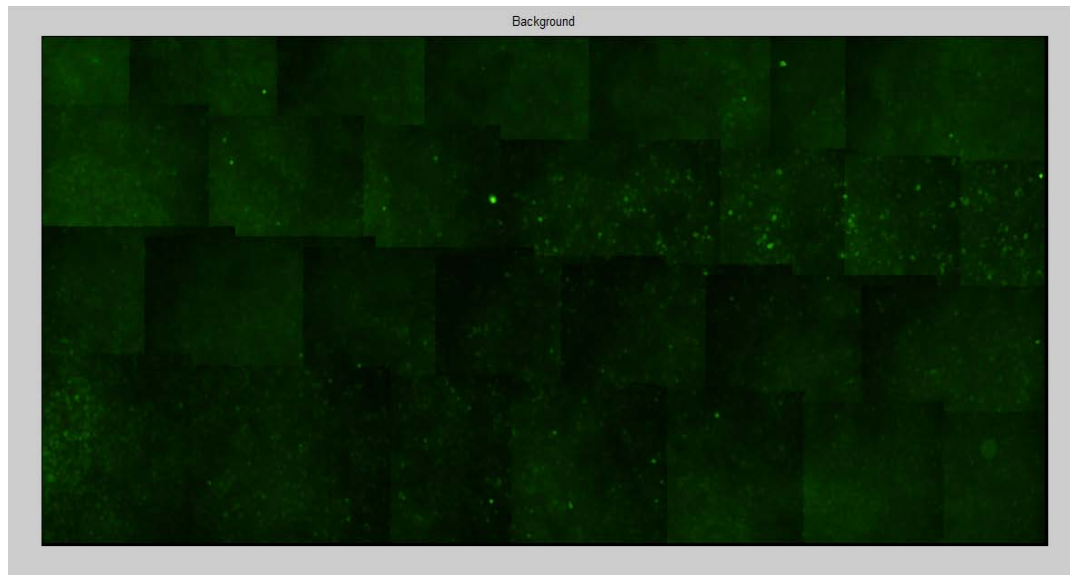


Figure 3.4 – The background image which had been subtracted from the image in Figure 3.2 (top) to create the image in Figure 3.3.2 (Bottom).

The ‘Background’ function employed the MATLAB operation *imopen(I,Se)* in which the ‘I’ variable represented the image and ‘Se’ was a single structuring element. To find ‘Se’ the MATLAB function *strel(Shape, parameters)* was used with the variable ‘Shape’, for the shape of the element, and ‘parameters’ representing the size of pixels allocated. The shape of the element was selected as ‘disk’ due to the similarity in the shape of the cells. Finally, the background image found from the *imopen(I,Se)* was created as shown in Figure 3.4. The background image displayed the inconsistencies between each individual image which had been pieced together as shown in Figure 3.4. Removing the inconsistencies from the original image reduced the noise within the image which could have hindered the analysis process.

3.3.3 Black and White Image

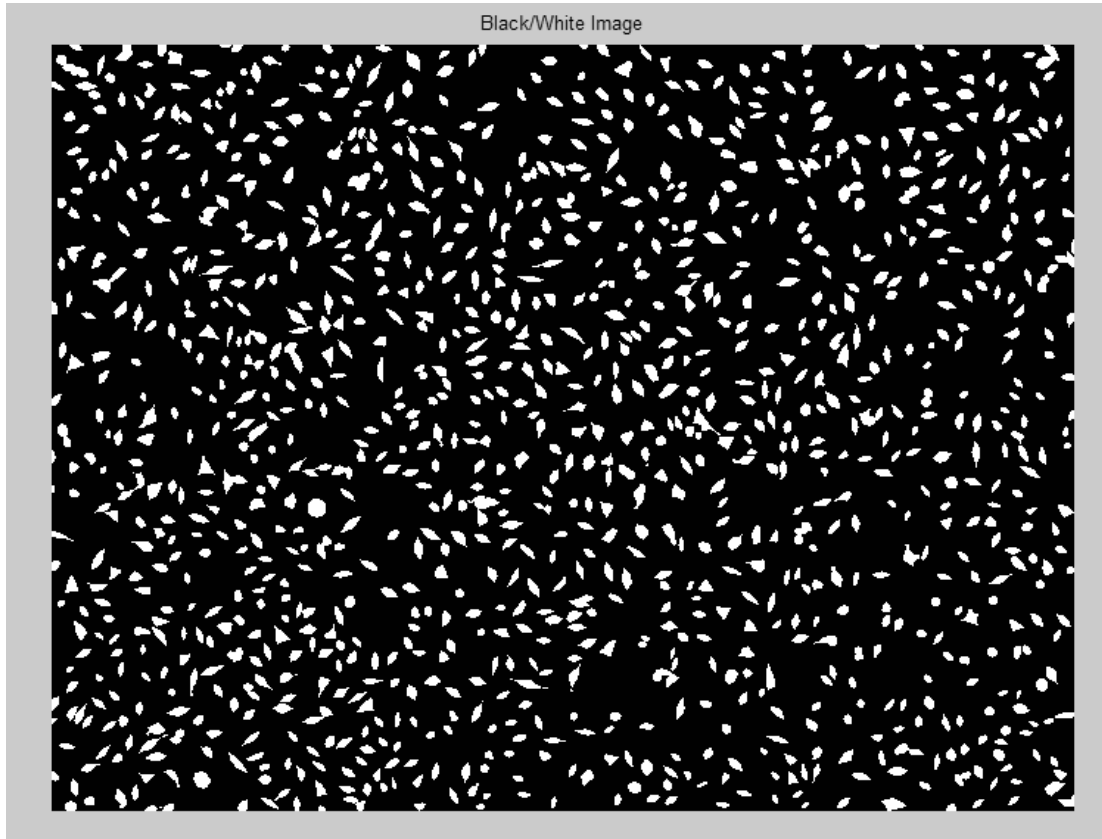


Figure 3.5 – ‘Black/White’ function of ImageGUI which converts the image into a black and white binary image.

The ‘Black/White’ function converted the image into a black and white binary image. The binary image had a lower file size than the colored image, but also has a lower resolution as well. The black and white images were easier to process than colored images due to their binary data.

The function consisted of the MATLAB operation *graythresh(I)* and utilized a global threshold of the image, ‘I’, through the use of Otsu’s method. The threshold value was used in the *im2bw(I,threshold)* MATLAB function to convert the image, ‘I’, into binary. In order to remove noise from the image which would be mistakenly labeled as cells, the function *bwareaopen(BW,size)* was used to remove artifacts below the set ‘size’ variable in pixels. The variable ‘size’ was determined by the individual cell size within the image.

3.3.4 Removing Border

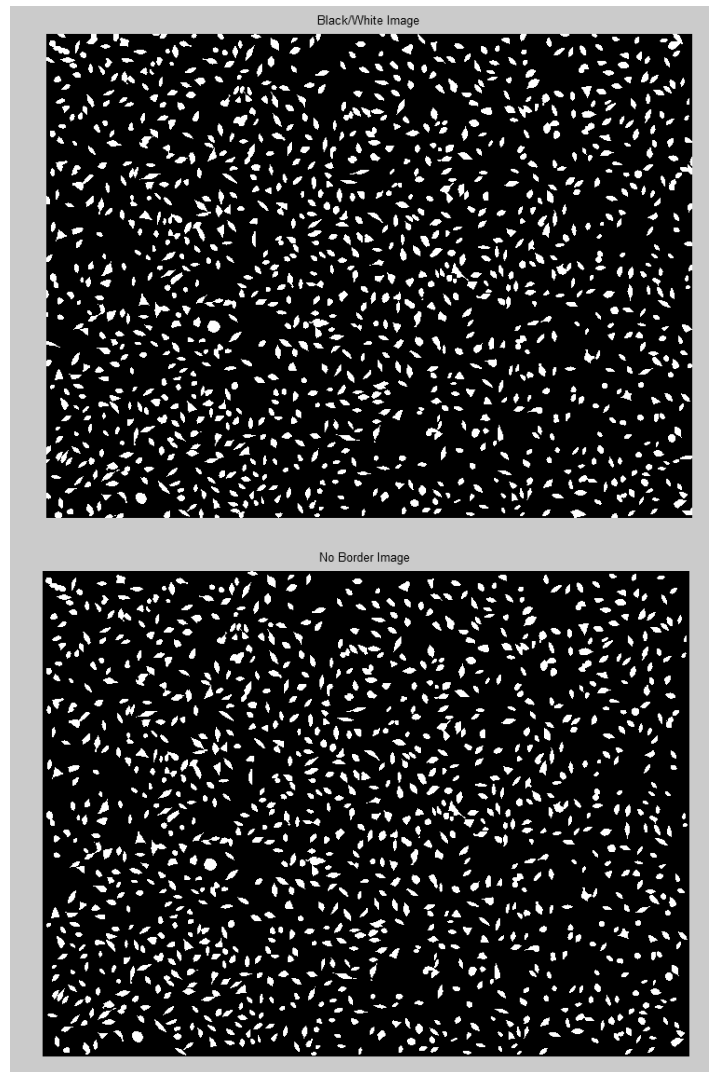


Figure 3.6 – ‘Remove Border’ function removed any cells which are located at the border and are not shown in their entirety.

The ‘Remove Border’ function removed any artifacts from the image which are located within 1 pixel of the border. The process purged cells which are not shown in their entirety and caused inaccurate results during the area and roundness analysis. The function utilized the MATLAB operation *imclearborder(I,conn)* with the ‘I’ representing the binary image and ‘conn’ allocating the size of the border. The ‘conn’ value was set to 4 to ensure each artifact within the image has four points of connectivity to the image

which was described in Figure 3.7. Artifacts on the edge of the image only had three points of connectivity and were removed.

A	B	C
D	E	F
G	H	I

Figure 3.7 – The ‘conn’ variable represented the connectivity of a pixel within an image. For example, the pixel ‘E’ has four points of connectivity: ‘B’, ‘D’, ‘F’, and ‘H’. Pixel ‘B’ however only has three points of connectivity: ‘A’, ‘C’, and ‘E’. This method eliminated any artifact which existed in contact with the border of the image.

3.3.5 *Smoothing Image*

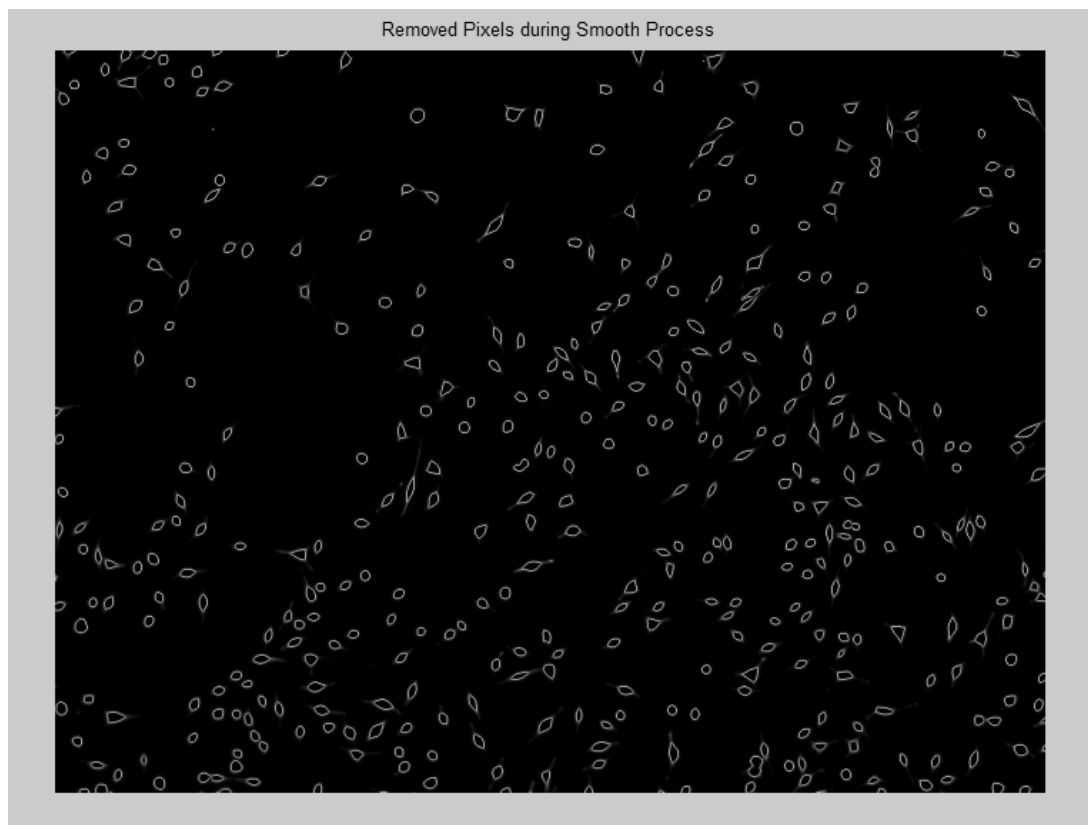


Figure 3.8 – The ‘Smoothing Image’ function removed the outline of the cells by a width of one pixel. The figure shows the portion of the cell which would be erased during the smoothing process. This method aided the counting cell process if the cell were in close proximity to one another.

The 'Smoothing Image' function removed a one pixel outline of each cell. The function was used to disconnect cells which have been connected through the binary process. Also, this function removed any small artifacts which had been added during the 'Back/White' function. The 'Smoothing Image' function was not used during the cell area and roundness analysis. In Figure 3.8, the portion which would be removed from the cells during the smoothing process was shown.

The MATLAB operation *imrode(I,SE)* was used with the variable 'I' representing the image and 'SE' representing a single structuring element found through the *strel*(Shape, parameters) operation. For the 'Smoothing Image' function the 'Shape' was set to diamond, and the 'parameters' variable was set to 1. The variable 'parameters' was set to 1 for the removing of 1 pixel around each artifact within the image.

3.3.6 Locating the Peaks

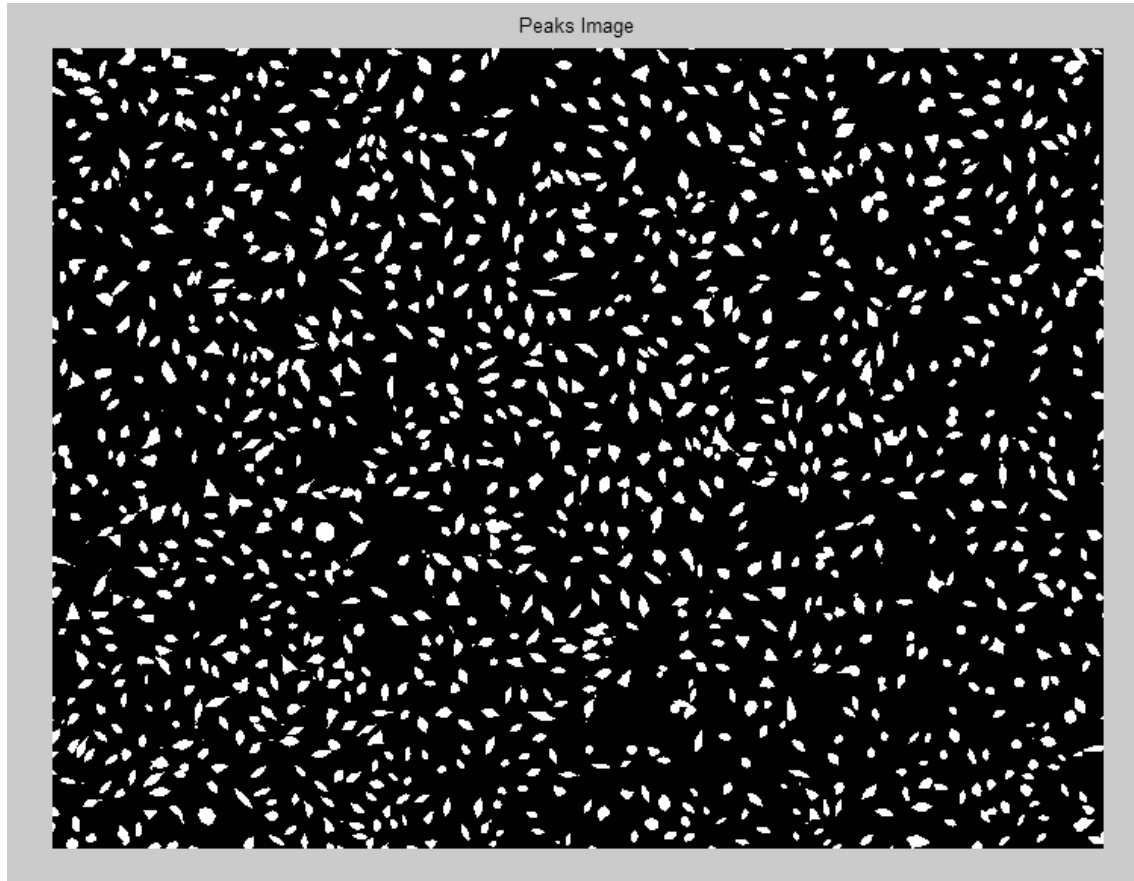


Figure 3.9 - 'Find Peaks' function located the pixels of common intensity above a set threshold within the gray image and connected them to form a binary image.

The 'Find Peaks' function located and connected the pixels which were above a set intensity threshold. The function utilized the *imextendedmax*(I,H) operation within MATLAB, in which 'I' was the gray image and 'H' variable was a scalar for the H-maxima transform. The 'H' variable was selected by the user, and for the cell images, the 'H' value was set to 100. The 'Find Peaks' function allowed the image to be converted to binary when the 'Black/White' function was not able to differentiate between the background and the cells.

3.4 Image Analysis Functions

ImageGUI has multiple functions for analyzing the images for cell count, area, and morphology after the image processing. After each analysis function, the data was saved in the MATLAB work space for further analysis. In order to use the analysis, the image had to be in binary form through the use of the 'Black/White' or 'Find Peaks' functions.

3.4.1 Cell Count

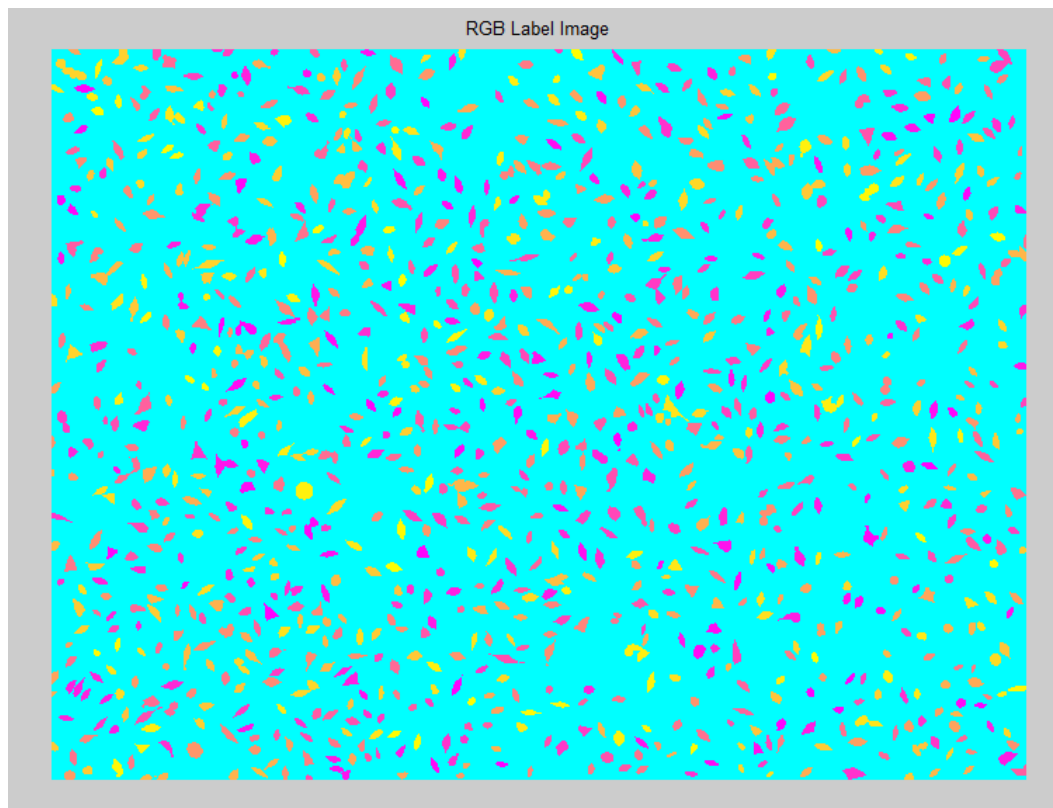


Figure 3.10 – The 'Count Cells' function created a multicolored image with each cell conveyed as a separate color to help in visually differentiating between cells in close proximity.

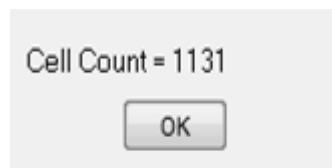


Figure 3.11 – The output window was designed to display the total number of cells in the image.

The 'Cell Count' function used the binary image to count each individual cell. A multicolored image was created to aid in differentiating the cells which were in close proximity to one another. The multicolored image helped the user identify cells in close proximity as to whether the cells were counted separately or as a single cell.

MATLAB located and labeled each cell within the image through the use of the *bwconncomp*(imag,conn) function. The *bwconncomp* function also allowed for the use of the *regionprops* functions which provided information about each cell's area, perimeter, major and minor axis lengths, and centroids. The centroids were used to find each cell's center of mass or location of the center of the cell.

The MATLAB function *label2rgb*(labeled,map,zerocolor,order) was used to count and label the individual cells by utilizing the variables, 'labeled' representing the binary image, 'map' to select the color scheme of the cells, 'zerocolor' for the background color, and 'order' to represent how the colors of each cell was selected. Variable 'map' was set to spring to give the cells colors ranging from purple to yellow, 'zerocolor' was set to 'c' to set the background as teal, and 'order' was set to shuffle to randomize the order of the cells' colors.

Validation of the MATLAB cell count function was done by comparing the software's output to a manual cell count. The main component impeding the software's analysis was the quality of the image. It was found that increasing the pixel quantity of the image would increase the accuracy of the count as seen in Figure 3.12 bottom.

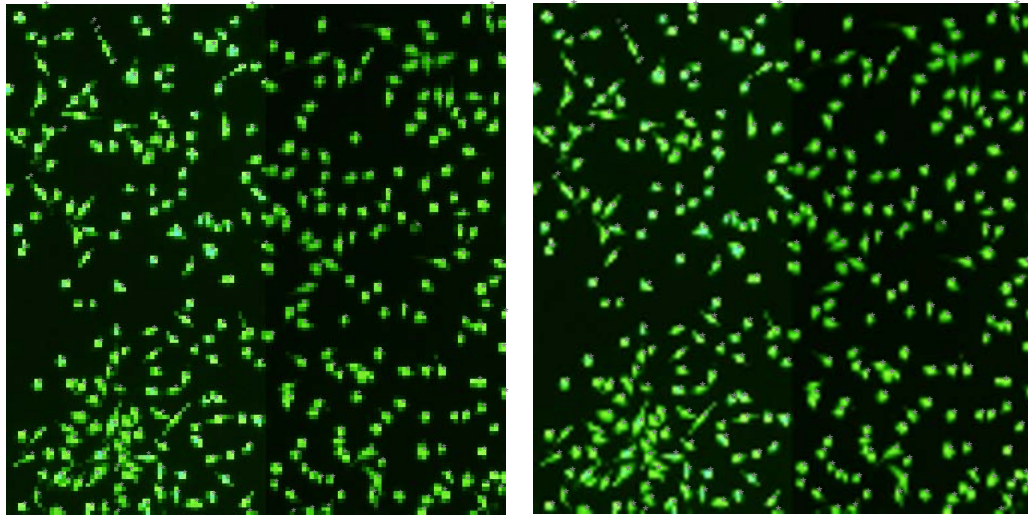
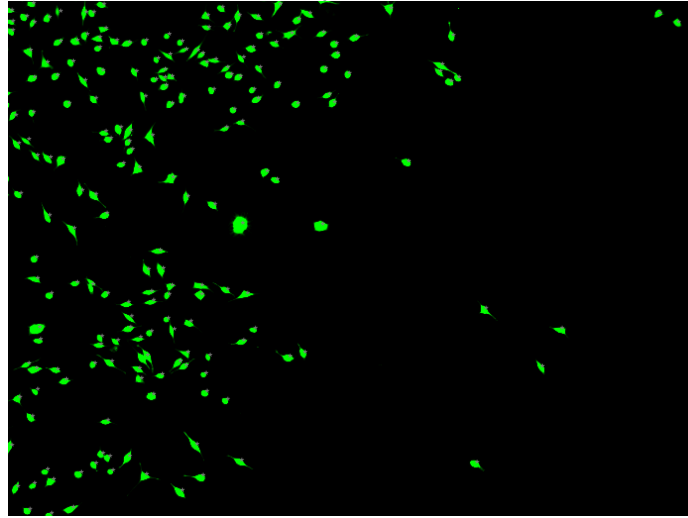


Figure 3.12– The MATLAB cell count function labeling the individual cells on the images during the counting process in order to compare the results with the manual counting results. The bottom images display the same image, but the right image has an increase in pixels per inch to demonstrate the affect of image quality on the software analysis.

In Figure 3.12, the top image's analysis provided counts of 200 cells during the MATLAB analysis compared to 202 cells manual analysis. The error in the cell count could be attributed to the two cells in close proximity, and the software was not able to differentiate resulting in the two cells being counted as a single cell. The bottom images were of lower quality due to the reduction of pixels per inch. The MATLAB cell count returned 332 cells while the manual count returned 334 cells. The quality of the image, pixels per inch, was increased before the manual count of the cells to ensure accuracy,

but was not increased during the MATLAB analysis. Ten errors in the MATLAB counting analysis were found with the counting of 4 non-existent cells and 6 missed cells. The mistakes of the uncounted cells occurred in areas where the cells were in close proximity. The errors in the counting software were not deemed significant due to the error percentage of 2.99%.

3.4.2 Cell Density Plot

The ability to impede the adhesion of fibroblast cells to a surface with the use of ultrasound was determined by examining the change in cell density of the vibrated and non-vibrated sections of the cell plate. The 'Cell Density' function displayed the cell density plot of the cell plate image. The function separated the image into 50×50 pixel sections, approximately 0.535 mm², to calculate the cell density values throughout the entire cell plate as seen in Figure 3.13. The number of cells within each section did not count the cells on the borders to ensure no cells were counted twice. The cell count of each grid was then plotted with a surface plot to create a cell density plot seen in Figure 3.14. The information of each grid cell count was also saved in the MATLAB workspace for further analysis of the data. The data for the surface plot was enhanced using the `interp2` function to increase the amount of data points for the visual inspection, but the data within the workspace was not affected.

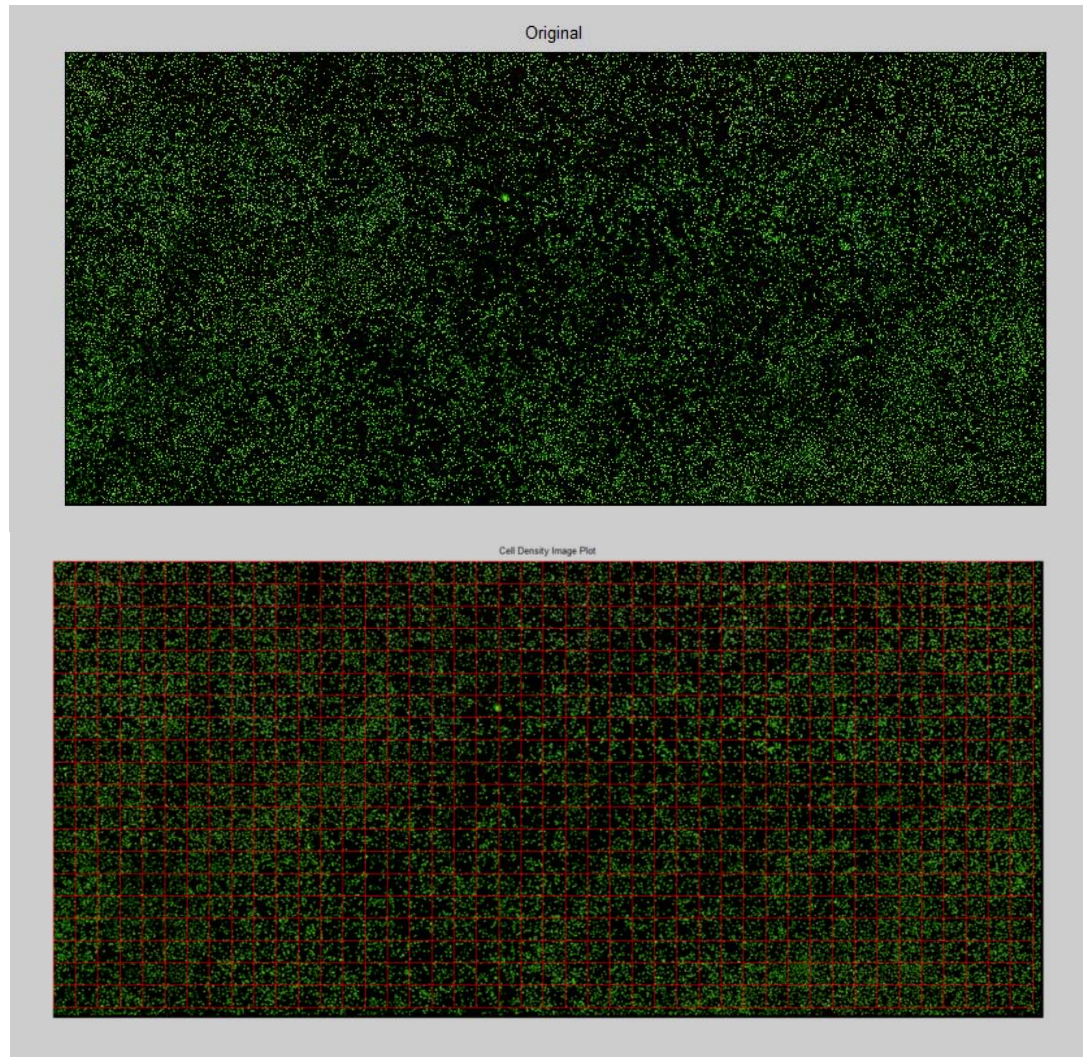


Figure 3.13 – The original image (top) was separated into 50×50 pixels sections, approximately 0.535 mm^2 , in MATLAB through the use of a grid. The cell density of each grid was calculated individually.

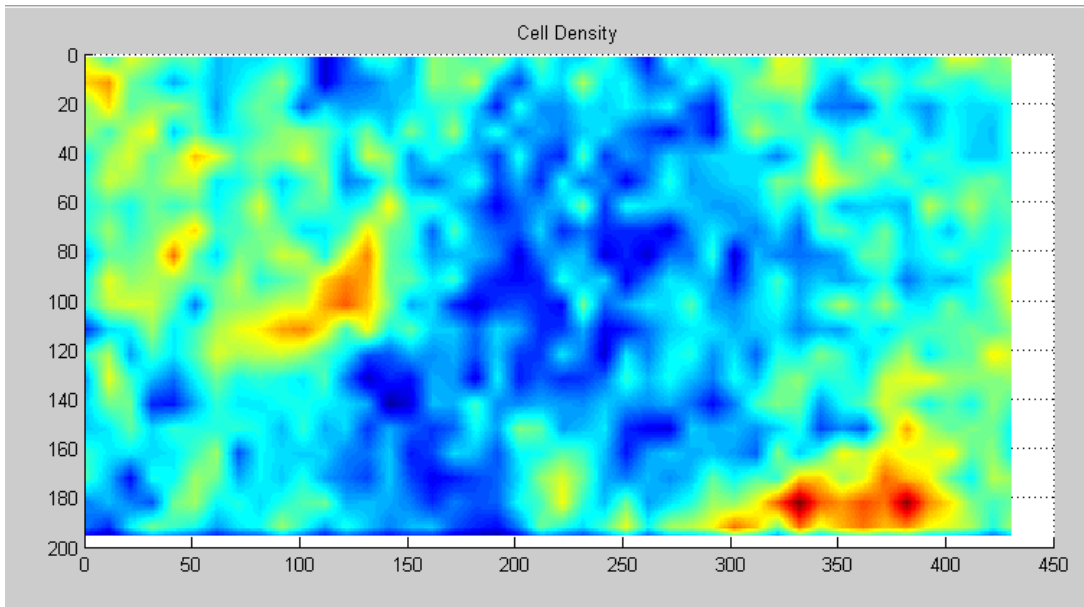


Figure 3.14 – The ‘Cell Density’ function calculated the cell density of the entire cell plate to aid in the cell detachment analysis. After each grid’s cell density was calculated, the information was plotted in MATLAB utilizing the surface plot function.

The cell density plot displayed a two dimensional representation of the cell density across the cell plate, and provided an illustration of any change in cell density between the multiple experiment trials. The plot also allowed for the comparison between the gel pad, and the cell density pattern shown on the cell density plate.

3.4.3 Cell Area

Cell morphology was a method to describe the adhesion strength of the cell to a surface. Cells with a stronger adhesion were believed to cover a larger area than weakly adhered cells [2]. Each cell’s area was found using MATLAB to determine the ultrasound’s effect on the cells’ adhesion.

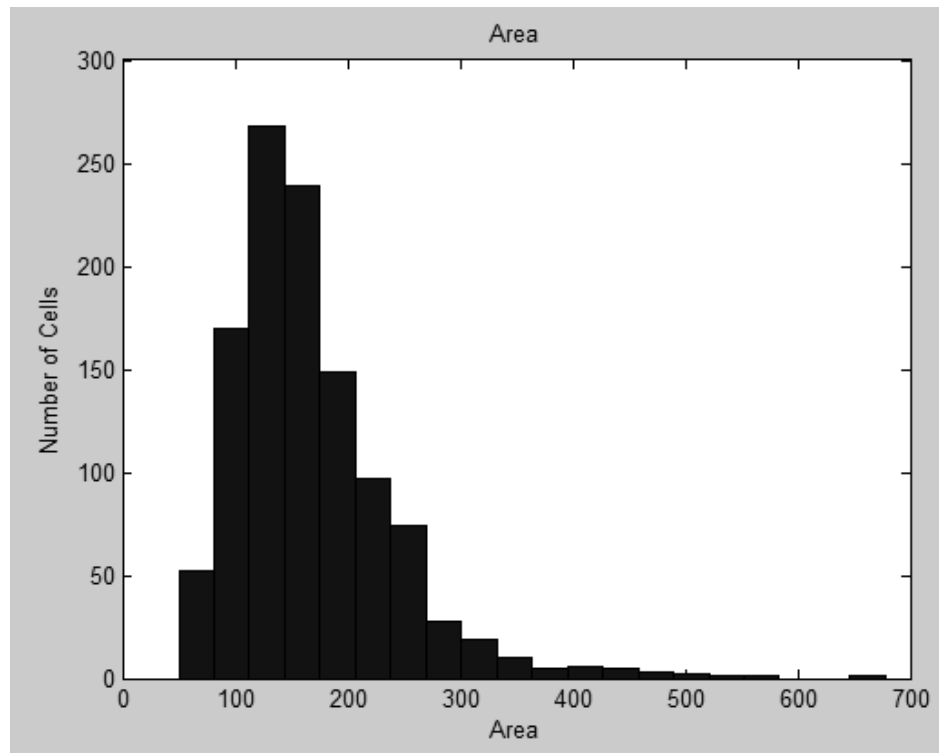


Figure 3.15 – The figure shows a histogram plot displaying the cell areas within the image below.

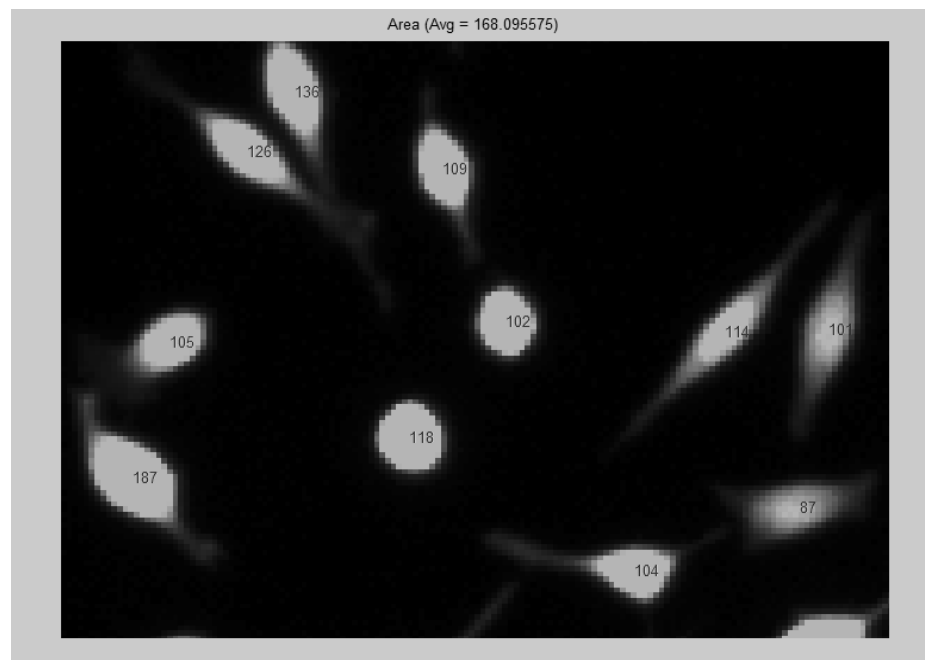


Figure 3.16 – Image of cells with the cell areas overlaying their corresponding cell.

The 'Cell Area' function calculated the area of each cell within the image in terms of pixels and saved the information to the MATLAB workspace under the variable 'area'. The data was also presented in a histogram plot along with the average area of the entire image shown in Figure 3.15. A dialog box presented the average, minimum, and maximum area of the cells. Finally, the data of the cells' areas were overlaid upon the image with their corresponding cell as seen in Figure 3.16. The overlay function allowed the user to manually locate each cell's area throughout the image.

The cell areas were found through the use of the *regionprops*(cc,'Area') operation in which 'cc' represented the stack of connected components within a binary image. The stack, 'cc', was found through the use of *bwconncomp*(I,conn) function, in which 'I' was the image and 'conn' was the connectivity. The cell area values were overlaid on the original image by using each cell's center of mass as a plot point.

3.4.4 Cell Roundness

In addition to the cell area, cell roundness was another method to describe the cell morphology. Cells which were strongly adhered to a surface achieved lower roundness values compared to the weakly adhered cells [2]. The function 'Cell Roundness' utilized the ratio between the length and width of each cell, in order to calculate the cell's roundness value. The data was also presented in a histogram plot along with the average roundness of the entire image. A dialog box presented the average, minimum, and maximum roundness of the cells within the image. Finally, the data of the cells' roundness' were overlaid upon the image with their corresponding cell as seen in Figure 3.18.

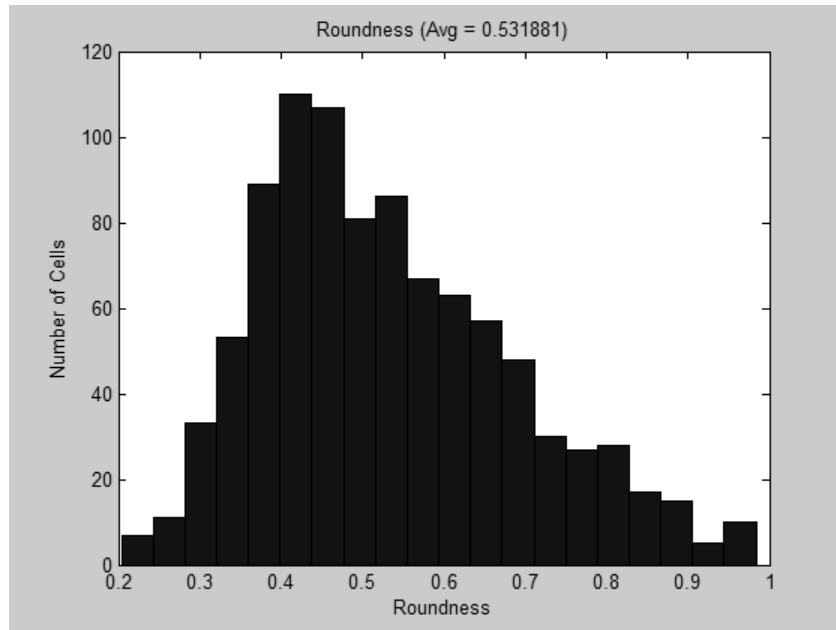


Figure 3.17 – Histogram plot of the cells' roundness through the image as well as the average roundness.

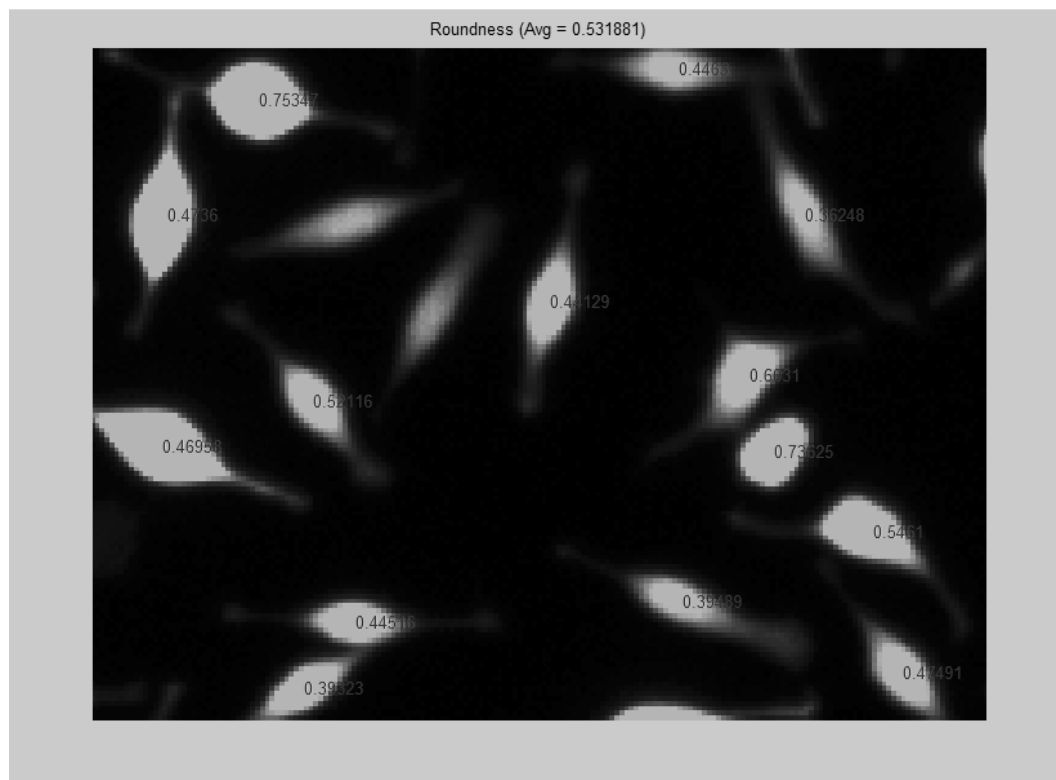


Figure 3.18 - Image of cells with the cell roundness overlaying their corresponding cell.

The cell roundness values for each image were found with the assistance of the *regionprops(cc,'MajorAxisLength')* and *regionprops(cc,'MinorAxisLength')* operations in which 'cc' represents the a stack of connected components within a binary image. The stack, 'cc', is found through the use of *bwconncomp(I,conn)* function, in which 'I' is the image and 'conn' was the connectivity. The 'MinorAxisLength' values were divided by 'MajorAxisLength' to find the roundness values for each cell. The cell roundness values were overlaid on the original image by using each cell's center of mass as a plot point utilizing the cell's centroid location.

3.4.5 Filter

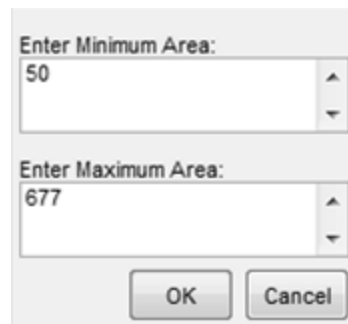


Figure 3.19 – The 'Filter' function was designed to allow the user to filter out cell areas by utilizing the desired minimum and maximum areas. The areas are in terms of pixels.

The 'Filter' function allowed the user to eliminate certain cells by utilizing the minimum and maximum areas desired for the analysis through the use of a dialog window. Small artifacts were sometimes introduced to the image during the black and white function and raising the minimum area erased those artifacts from the data. Also, some cells in close proximity were joined together in the image processing and formed a single cell with a large area. Both of these incidences were corrected through the use of the 'Filter' function. The function employed a comparison operation to eliminate values outside the limits set by the user. The new data was then stored in the ImageGUI program and in the workspace.

4. Experiments

Fibrosis has the ability to cause implanted devices to malfunction and potentially harm the patient. Fibroblast cells are the main type of adhesion cells in the encapsulation process and isolate the implant from the biological environment. Fibroblast adhesion has been shown to be affected through the use of a mechanical stimulus. Controlling cell adhesion through the use of an in-vivo ultrasound treatment has the ability to enhance the antifouling effect of implanted devices. Experiments were completed to test the ultrasound's effect on the fibroblast adhesion properties by analyzing the change in the cell viability, cell density of the plate, and cell morphology.

4.1 Materials

All cells utilized in the experiments were L929 fibroblast. The culture medium consisted of 10% fetal bovine serum (FBS), 0.5% ATCC Penicillin-Streptomycin in Dulbecco's Modified Eagles Medium D5796 with 4500 mg glucose/L, L-glutamine, NaHCO₃, and pyridoxine. The cells were washed with phosphate buffered saline (PBS) with 0.53-mM ethylenediaminetetra acetic acid (EDTA). Trypsin-EDTA was used to detach the cells from the tissue culture dishes. Calcein-AM fluorescent and Ethidium Bromide dyes were used to stain the fibroblast cells for live and dead analysis. 35 mm × 12 mm polystyrene tissue culture dishes were purchased from BD-Falcon to ensure adequate surface area for the ultrasound transducer. Images of the cell adhesion were taken from a Leeds Olympus BX51 microscope. A 14 mm × 1 mm gel pad, Aquaflex Ultrasound Gel Pad, was used to facilitate the transfer of ultrasonic energy to the cell dish. An ultrasound gel pad was used in the replacement of fluid gel to ensure a consistent pattern is obtained for each trial.

4.2 Fibroblast Cell Passage Protocol

Cell media was aspirated from the culture plate. The cells were washed with 5 mL of sterile PBS to remove the residual serum and then aspirated again. The addition of 5 mL of Trypsin to the cells and the incubation of the cells at 37° C for 2-5 minutes

detaches the cells from the culture plate. The Trypsin was deactivated by 1 mL of PBS. The cell solution was transferred to a flask and placed in a centrifuge at 1000 rpm for 5 minutes in order to create a cell pellet. The excess solution was aspirated, and 6 mL of media was added to disperse the pellet. A cell count was performed to ensure the correct cell seeding density is obtained. The cells were separated into the four tissue culture dishes at a density of 1.3×10^4 cells per cm^2 to ensure a consistent cell density on the plate, and then the cells were incubated for 48 hours at 37°C .

4.3 Ultrasound Procedure

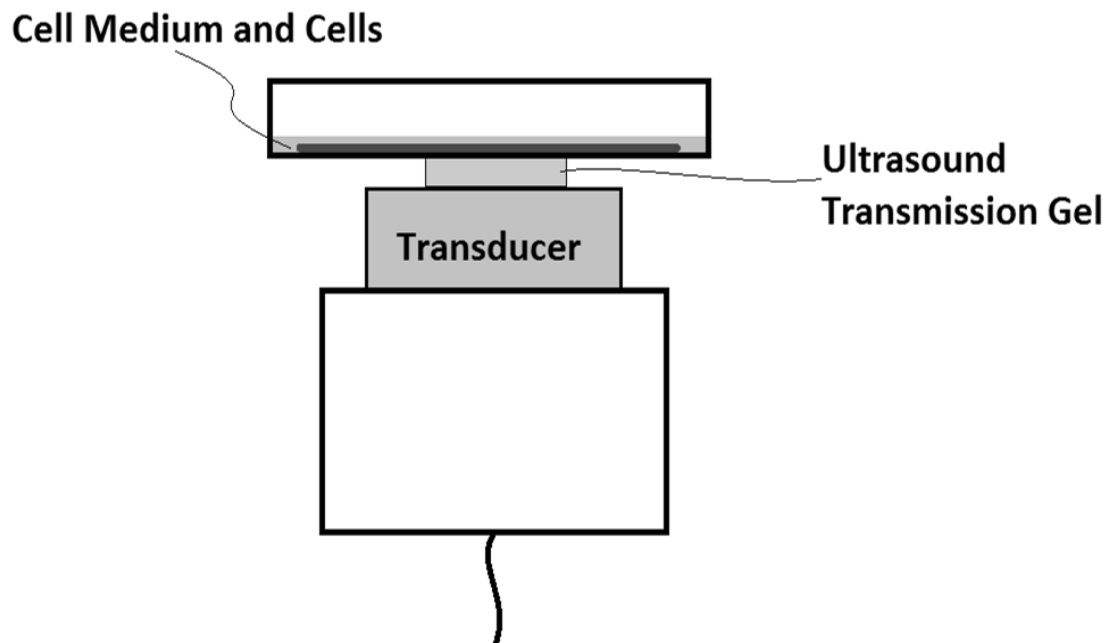


Figure 4.1 – Ultrasound transducer setup for cell experiment with the ultrasound transmission gel place in the middle of the cell plate.

The four cell tissue dishes were transferred to the incubator in which the ultrasound experiment was performed, with each sample placed on the same platform to ensure consistency. The Aquaflex Ultrasound Gel Pad was placed in between the ultrasound transducer and aided the transfer of the ultrasonic energy to the cell plate. The size of the gel pad used was 14 mm in diameter to create a surface area large enough to ensure stability of the plate throughout the experiment. The cell samples were placed,

one at a time, on the ultrasound transducer to perform each trial. The ultrasound transducer outputted a 1 MHz signal a predetermined intensity for 1 hour each trial. The ultrasound intensity on the cells was set to -25 dBm, -22 dBm, and -21 dBm for the trials 1, 2, and 3 respectfully.

4.4 Staining Procedure

Once the ultrasound procedure was completed, the samples were stained for the live and dead analysis. A flask was used to create the staining solution consisting of 10 mL of PBS, 10 μ L of Ethidium Bromide, and 5 μ L of Calcein-AM. For each cell dish, 2 mL of staining solution was added and incubated for 20 minutes then aspirated. The samples were then analyzed utilizing the upright Leeds Olympus BX51 microscope.

4.5 MATLAB Analysis

The analysis on the cell plate images was done using the MATLAB image processing tools. The processing method on the images was determined by the type of analysis which would be required.

4.5.1 Cell Viability

Two images of the cells were taken by the fluorescent microscope for the cell viability analysis. One image was taken for the live cells with the Calcein staining, and the other image was taken for the dead cells with the Ethidium Bromide staining. The images were overlaid upon each other with the assistance of MATLAB to create a full image of the area. The images were also analyzed individually for a cell count to determine the ratio of live to dead cells within the area.

4.5.2 Cell Density

The images of the cells were assembled together with the use of Microsoft Paint to create a full image of the cell plate. The assembled image was processed using MATLAB to create a binary image in order to perform the cell count analysis. The 'Cell Density Plot' was used to create a surface plot of the cell density throughout the cell plate

by creating 50×50 pixel sections throughout the image. The data was saved in the MATLAB workspace under the variable, *Density*. A plot of the densities within each section was created to show the relationship between the vibrated and non-vibrated sections of the plate.

4.5.3 Cell Morphology

Separate images within the vibrated and non-vibrated section of the cell plate were used to analyze the cell morphology between the two sections. The images were converted into binary before being analyzed for area and roundness. The ‘Filter’ function was used to eliminate any cells which were conjoined during the image processing. Finally, a histogram plot was used to display the distribution of the cell morphologies within the image.

4.6 Statistical Analysis

The experiments were completed three times in order to collect data for quantitative analysis. The data analysis was performed using the variance (ANOVA) with a standard t-test. P-values of < 0.05 were considered significant, and error bars used on graphs were representative of the standard error of the mean (\pm SEM).

5. Results and Discussion

5.1 Cell Viability

In order to determine the effect of ultrasound has on the cell viability, a fluorescent live-dead stain was used to compare the vibrated and non-vibrated areas of each plate. The cell viability results displayed the relationship between the ultrasound intensity and the death of the cells. Death of the cells could occur due to the ultrasonic compressive wave rupturing the cell membrane or by the altering of the cells' nutrient intake and activating their apoptosis response. The cell plates were stained with Calcein-AM and Ethidium Bromide for live-dead analysis. The cells were imaged utilizing fluorescent microscope to obtain images of the live cells and another image for the dead cells. The two images were overlaid upon on another to complete the live-dead analysis.

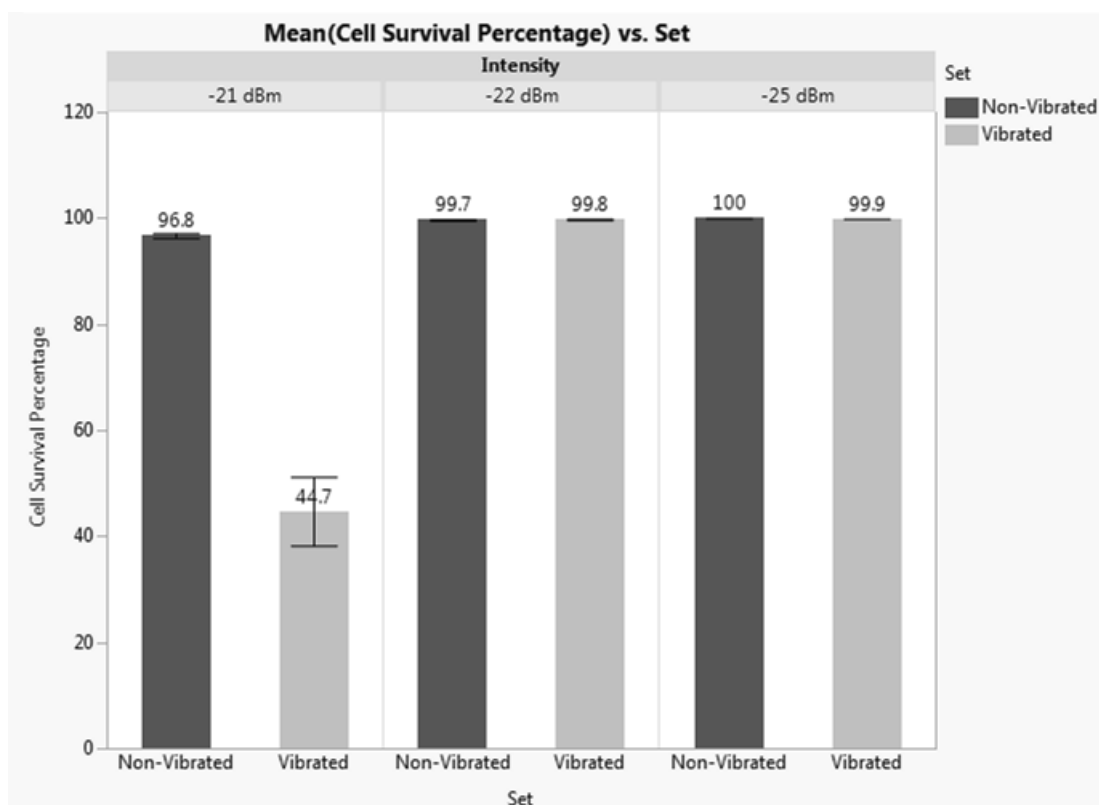


Figure 5.1 – Quantitative results of the percentage of cell survival (n=3 for each group). Statistical analysis was made using ANOVA with a standard t-test, and p-values <0.05 were considered significant. The error bars represent the \pm SEM. The -21 dBm trials showed significant loss of cell survival compared to the other two trials (p-value < 0.001).

For the -25 dBm trial, as well as the -22 dBm trial there was no change in cell viability throughout the cell plate as shown in Figure 5.1. For -21 dBm, the non-vibrated area of cell plate was consistent with the -25 dBm and -22 dBm tests. However, the center of the vibrated portion consisted entirely of dead cells with a sparse amount of live cells around the gel border. Outside the gel pad, the vibrational intensity sharply decreases, allowing for a defined edge of the cell viability.

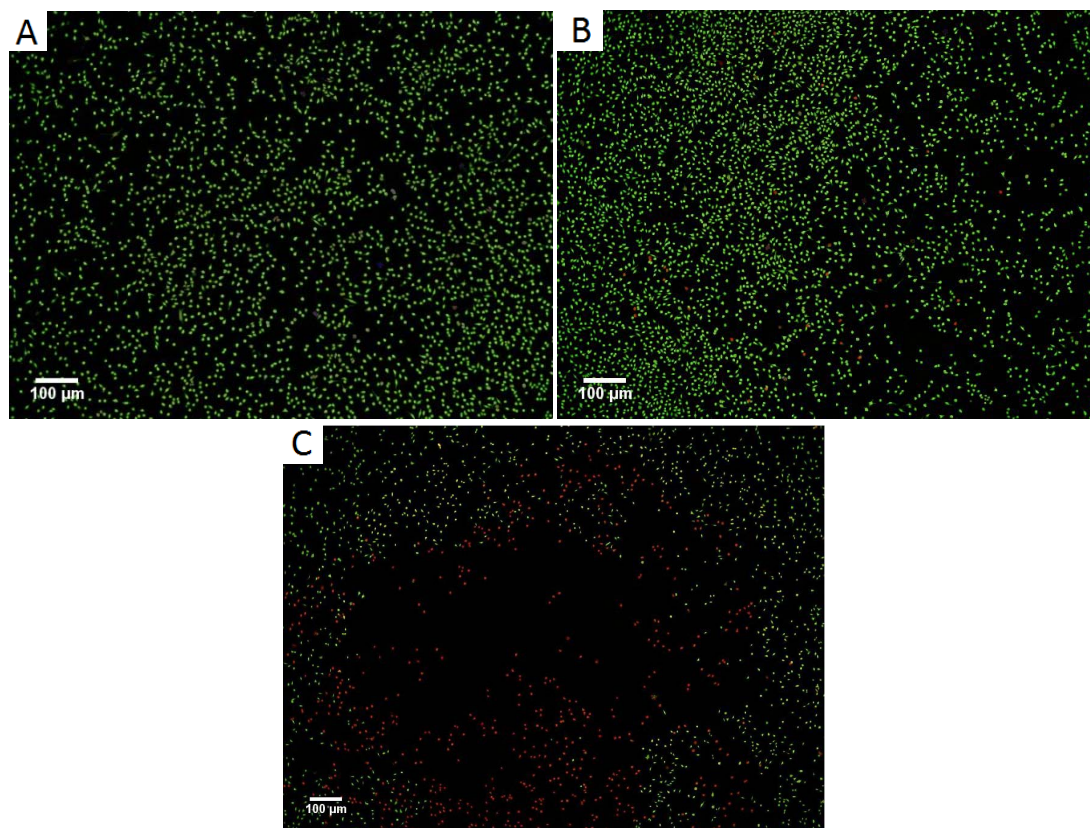


Figure 5.2– Cell viability of the three ultrasound cell trials. The -25 dBm (A) and -22 dBm (B) images showed no signs of dead cells attributed to the ultrasound treatment. The -21 dBm (C) image did show the area of dead cells within the center of the targeted area.

In Figure 5.2, Image (C) shows the -21 dBm trial with dead cells in the vibrated portion, but more live cells appear as the distance from the vibrated portion becomes greater. The cause of the shift from dead cells to live cells is due to the lowering of the ultrasound intensity as the plate transitions off of the gel. The shift from live to dead cells in the treated area allows for a description of the relationship between cell viability and ultrasound intensity. Image (A) shows the non-vibrated cells on the bottom right and the vibrated section is on the left. Image (B) has the vibrated section on the right and the non-vibrated on the left.

Cell death can arise through two different methods, necrosis and apoptosis. Cell necrosis is a premature death of a cell from external stimulus which results in damage to the cell membrane and causes an inflammatory response within the biological system. Cell apoptosis is the process of the cell dismantling its internal structures in order to be

removed by phagocytes. Apoptosis does not result in an increase in immune response and would be beneficial to the treatment [21].

The cell death in -21 dBm trials was the result to the low intensity ultrasound treatment. Previous study have shown that the ultrasound treatment at low intensity was due to apoptosis of the cell, but there was a difference in treatment time length compared to the trials in this experiment [22]. Due to those previous studies, it is believed that the cell death within the -21 dBm trials was the result of the apoptosis process. This result would be beneficial to the treatment to remove the fibroblast cells without increasing in the inflammatory response. Further testing would be required to prove this theory such as staining the cells with an apoptosis pre-marker.

5.2 Cell Density

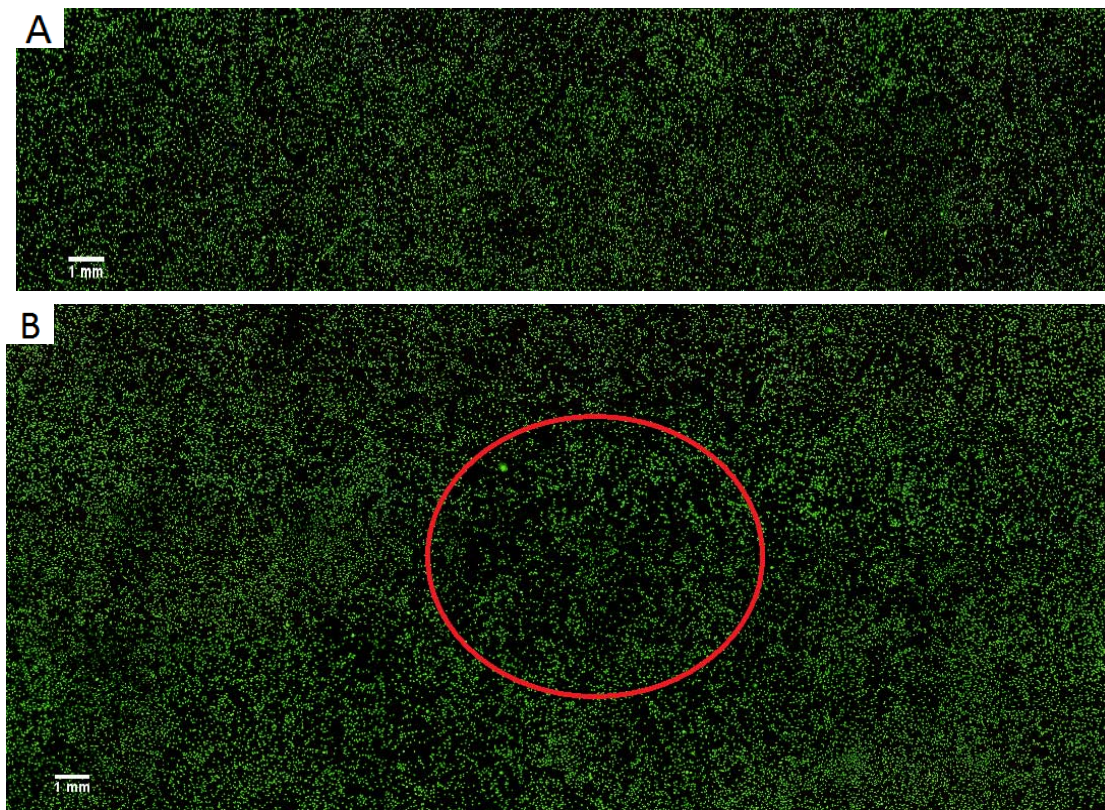
Cell density provided information on cell detachment in response to the applied vibrations. The ability to characterize the detachment of fibroblast cells within the targeted area allows for the ability to create a model for controlling the fibrotic adhesion response with the ultrasound treatment. The cell density of the non-vibrated section was compared to the vibrated section, as well as the change of density in relation to the distance from the gel placement. The cell density was calculated by analyzing 50×50 pixel sections, approximately 0.535 mm^2 , of the vibrated and non-vibrated areas on the cell plate and calculating the density of live cells.

Table 5.1

The table displays the average cell density of 50×50 pixel sections, 0.535 mm^2 , for vibrated and non-vibrated sections. The increase in the non-vibrated section cell density is due to the reattachment of cells at the gel perimeter after they detached from the targeted area.

	Power	Cell Density (cells/ 0.535 mm^2)	
		Vibrated	non-Vibrated
Control	-110 dBm	N/A	43.500
U2	-25 dBm	29.600	41.500
U3	-22 dBm	26.100	51.800
U4	-21 dBm	7.000	40.800

A non-vibrated control was used to determine the cell density of a non-vibrated cell plate and utilized to compare the results with the non-vibrated sections of the vibrated cell dishes. The control, shown in Table 5.1, was found to have a density of 43.5 cells per 0.535 mm^2 , which was consistent with the non-vibrated sections of the -25 dBm and -21 dBm trials, at 41.5 and 40.8 cells per 0.535 mm^2 respectively. The control's cell density was higher, but this result could be attributed to the resonance vibration which was spread across the entire plate during the ultrasound treatment. The non-targeted sections did receive a weak vibration from the ultrasound because of the cell plate being a rigid surface. Trial -22 dBm had a higher density of 51.8 cells per 0.535 mm^2 due to the increase of cells around the edge of the gel pad as seen in Figure 5.3C.



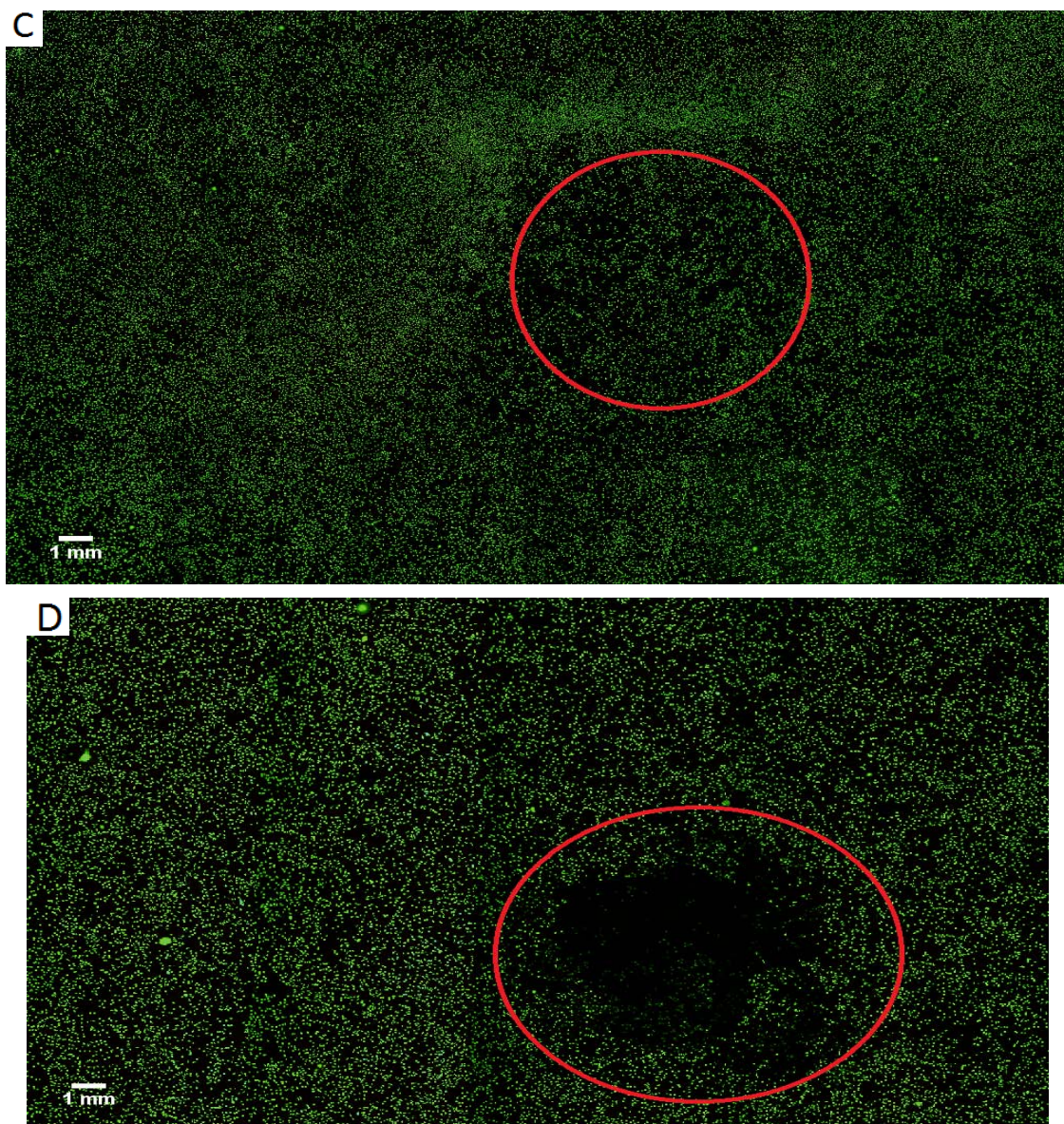


Figure 5.3 (A-D) – Images of the control and three ultrasound trials taken with the microscope of the entire cell plates. **(A)** - The control plate with no ultrasound treatment added to the cell plate. **(B)** - The -25 dBm trials with the approximate targeted location highlighted by the red circle. **(C)** - The -22 dBm trial with the approximate targeted location highlighted by the red circle. **(D)** - The -21 dBm trial with the approximate targeted location highlighted by the red circle.

The vibrated sections of the cell dishes showed a similar pattern in the detachment of cells in the -25 dBm and -22 dBm trials with densities of 0.592 and 0.522 cells per 0.535 mm^2 , but considerable detachment was seen in the -21 dBm trial with a density of

0.140 cells per 0.535 mm². The center of the vibrated portion in the -21 dBm trial did consist of dead cells which were not included in the density calculation.

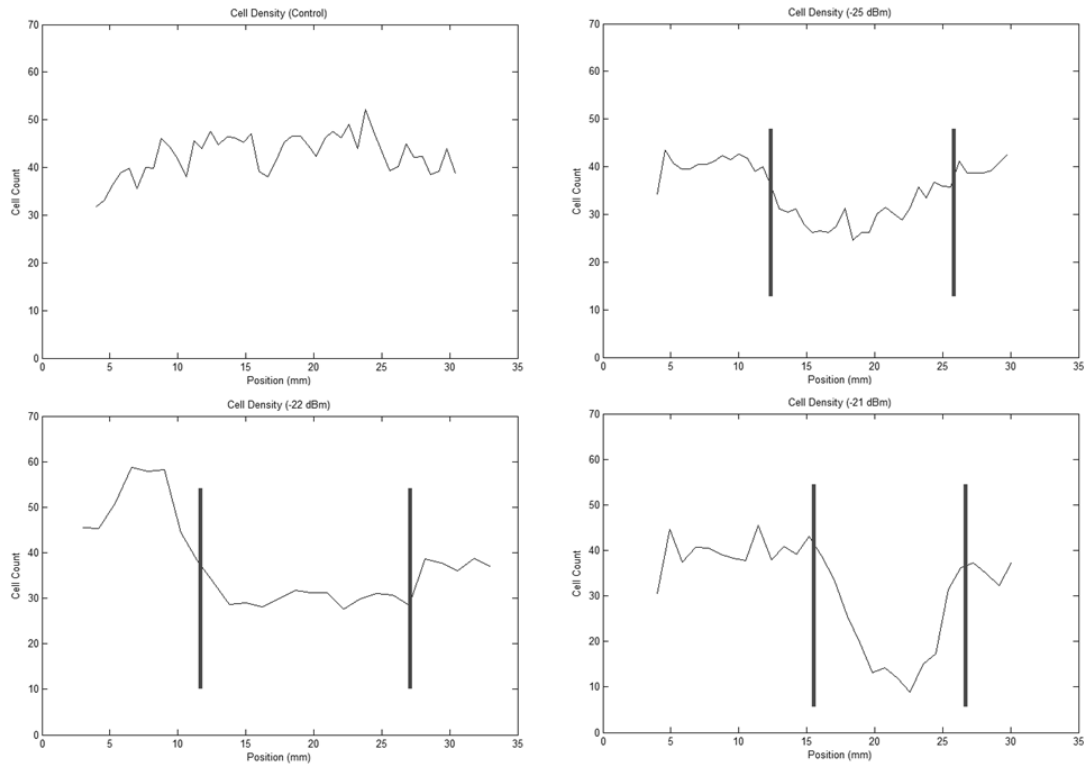


Figure 5.4 – Cell densities throughout each of the cell plates. The position is location in respect to the plate. In the -22 dBm trial, a large increase in cell density was seen around the 2 mm to 8 mm region of the plate unlike the other trials due to cell migration. The -21 dBm trial showed the greatest amount of cell detachment within the target area, but a significant amount of dead cells were also present. The approximate border is marked on each of the plots.

Unlike the -25 dBm trial, the -22 dBm trial showed an increased cell concentration found in the 2 mm to 8 mm section of the plate shown in Figure 5.4. The cell plate was placed on an uneven gel pad causing the detached cells from the vibrated section to migrate to the non-vibrated section and reattach. The -25 dBm trial was on a similar uneven gel pad but did not experience cell migration due to the lower intensity not fully detaching the cells from the plate. Majority of the cells were only fully detached after the PBS wash during the staining procedure. The -21 dBm trial had cell detachment but did not experience cell reattachment due to the death of the cells within the targeted area.

The results from the detachment of fibroblast cells within the targeted area allowed for the ability to create a model of the ultrasound treatment. The results in Table 5.3 and Figure 5.4 showed a correlation between the increase in the intensity of the ultrasound and the increase detachment of the fibroblast cells. In Figure 5.4, the -22 dBm trial displayed results with cell migration and reattachment to areas of non-vibration, unlike the -25 dBm trial in which the cells did not migrate or fully detach until the PBS wash during the staining procedure. The results would signify that the -22 dBm trial produced greater evidence for use in the removing of the fibroblast cells from the targeted region without the aid of an added shear force.

5.3 Cell Morphology

The difference in the morphology of cells between the vibrated and non-vibrated sections, in addition to the control plate, was used to represent the effect that ultrasound has on the cell adherence. Cell morphology was characterized by two methods: the ratio of the length versus width of each cell to determine their roundness ratios and the area of the cell to determine their adhesion spreading capabilities [2]. These methods were used to determine the cells which did not detach from the surface of the plate due to the vibrations. A comparison between the cells in the targeted region and the non-targeted region were made to determine the effect of the ultrasound treatment.

5.3.1 Cell Roundness

The cell roundness ratio allowed for the characterization of the adhesion properties of the cell. Cells which were more strongly adhered to the surface become elongated while lightly adhered cells were believed to be more round [2]. In order to find the roundness values of the cells, the length and width of the cells were found. The length of the cell was determined as the largest distance from the center of the cell to the cell's edge, and the width was determined as the shortest. Average roundness of the cells was evaluated for sections of the vibrated and non-vibrated areas in the cell plates. The control was found to have an average roundness of 0.6336, which was used for comparison to the non-vibrated areas of the three trials. The -25 dBm, -22 dBm, and -21

dBm trials had non-vibrated sections with a higher roundness ratio due to the vibration energy transferred throughout the entire plate, but not enough energy to completely detach the cells.

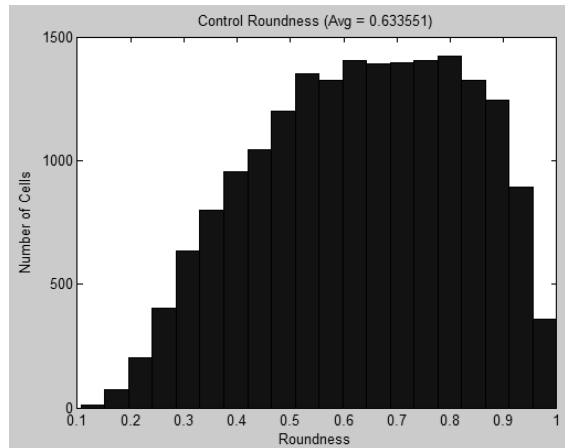


Figure 5.5 –The roundness of the Control samples with no vibration added to the cells.

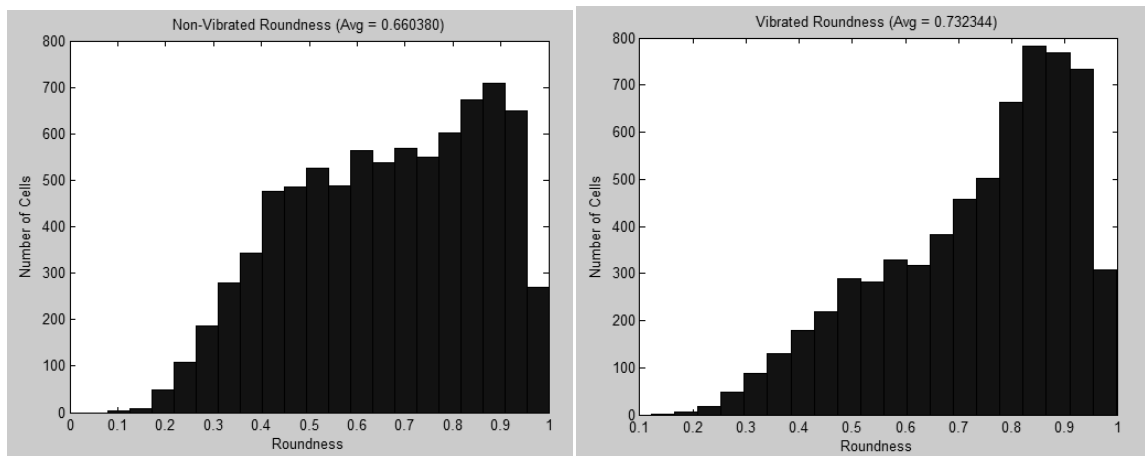


Figure 5.6 – The roundness of the cells in the -25 dBm samples with the non-vibrated section (left) and the vibrated section (right).

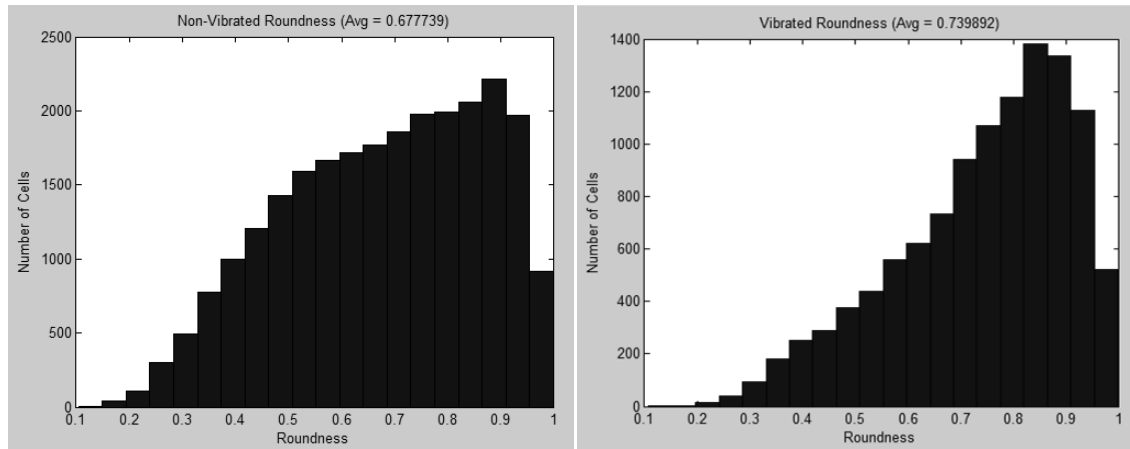


Figure 5.7 – The roundness of the cells in the -22 dBm samples with the non-vibrated section (left) and the vibrated section (right).

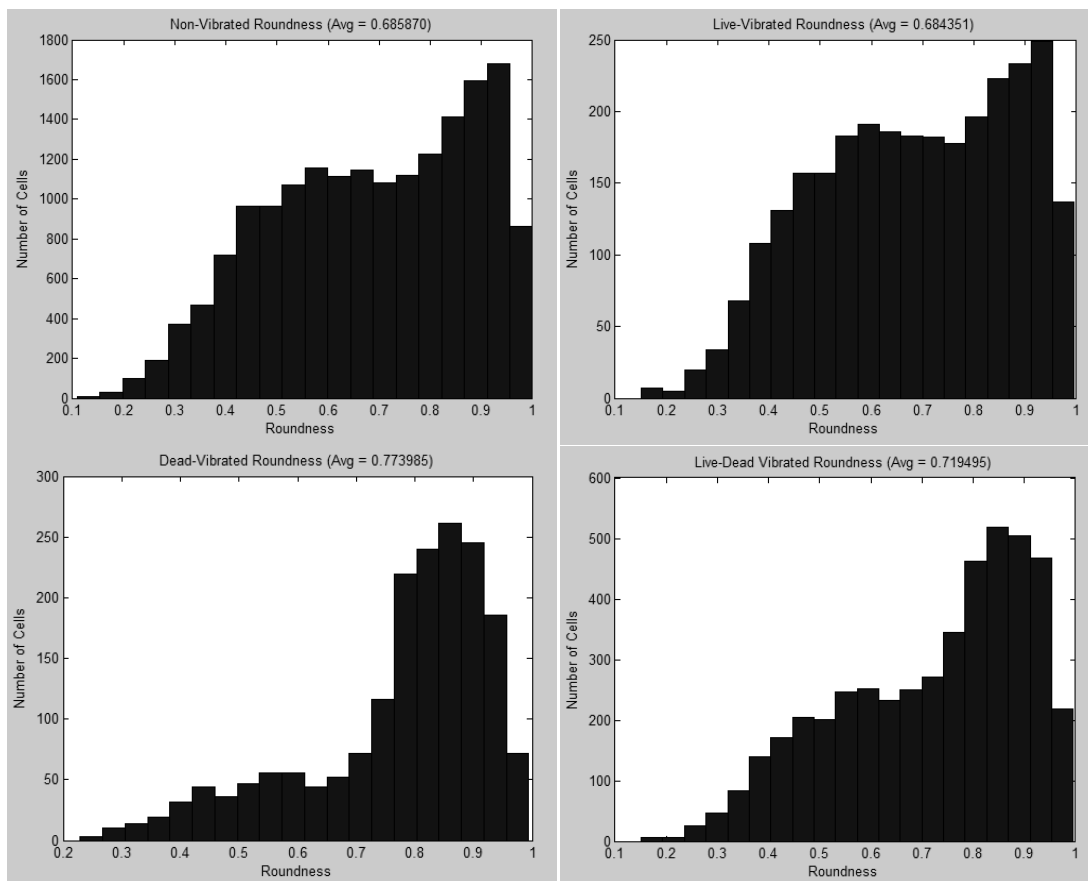


Figure 5.8 – The roundness of the cells in the -21 dBm samples with the non-vibrated section (top left), the live cells of the vibrated section (top right), the dead cells of the vibrated section (bottom left), and the entire live-dead section of the vibrated section (bottom right).

The average roundness values for the non-vibrated portions of the cell plates in the -25 dBm, -22 dBm, and -21 dBm samples were 0.6604, 0.6777, and 0.6859, respectfully. The increasing in roundness could be attributed to the ultrasound intensity vibrating the entire cell plate and affecting the cells outside the targeted area.

The roundness values were higher for the vibrated sections in the -25 dBm and -22 dBm samples which portrayed the ultrasound's effect on the adhesion of the cells. For the -21 dBm trial, the cells in the non-vibrated section and the live cells in the vibrated section had similar roundness values at 0.6859 and 0.6844 respectfully. The similarity was due to the live cells residing mainly on the edge of the gel which did not receive a high enough ultrasound intensity to change their morphology. The number of live cells in the target area was reduced due to most detaching or being killed by the ultrasound, and the remaining only cells were the ones more firmly attached. The dead cells in the vibrated section had an average roundness value of 0.7740 and the average of all of the cells in the targeted area was 0.7195, which was an increase to the non-vibrated section of the plate. The low cell density of the targeted area could also reduce the roundness value due to the detachment of the cells in the PBS wash during staining. The cells with the higher roundness values were believed to not be adhered strongly enough to withstand the PBS wash and resulted in a lower average roundness.

The increase in roundness of the cell morphology within the targeted areas shows the ultrasound's effect on cell adhesion. The cells were not able to maintain their adhesion to the surface of the cell plate in the presence of the vibrations. The result portrays that even if the cells were not fully detaching form the surface, their adhesion capabilities were affected.

5.3.2 Cell Area

The cell's area allowed for the characterization of the adhesion properties of the cell to a surface. A cell which was strongly adhered to the surface would broaden its structure across an section and increase its area [2]. The area of the cell was found by counting the pixels of a cell within an image. Images were separated into two groups, vibrated or non-vibrated, and the area of each cell was found. The cell areas were then

recorded to determine the mean and standard error of each trial and were shown in Figure 5.9. In each of the trials, only the area of the live cells was used in the calculation while the area of the dead cells was discarded.

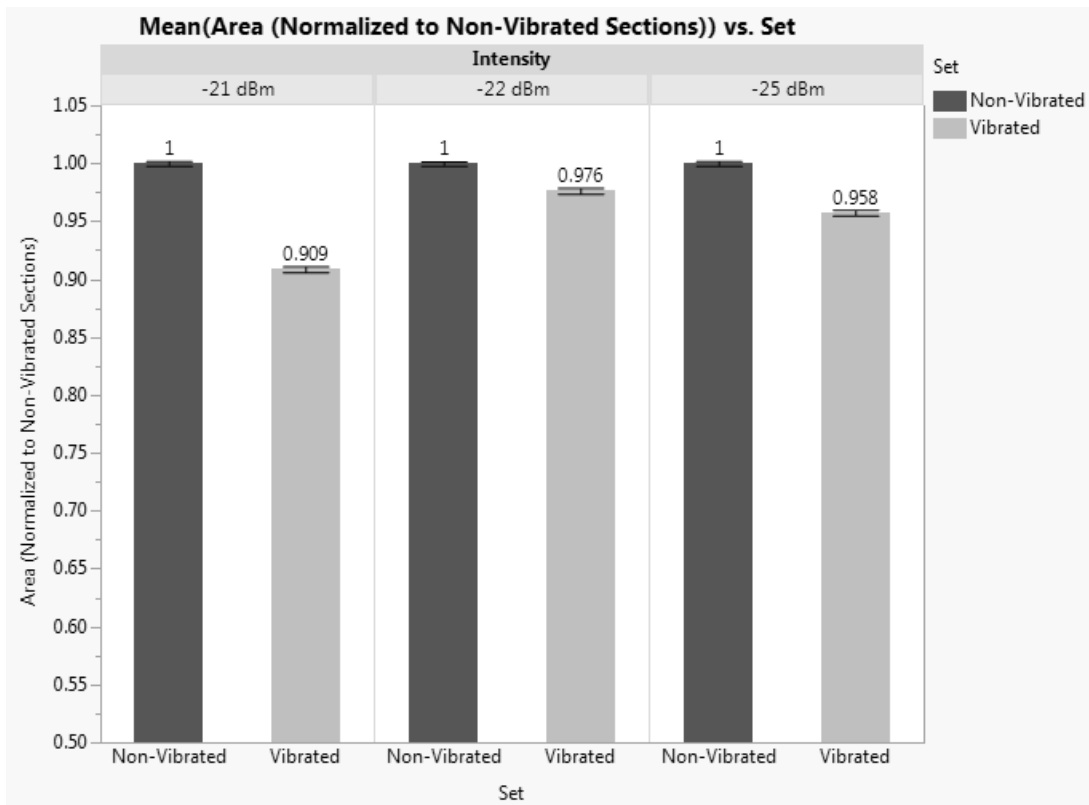


Figure 5.9 - Quantitative results of cell area with the mean of the areas normalized to the non-vibrated regions of the corresponding plate (n=3 for each group). Statistical analysis was made using ANOVA with a standard t-test and p-values <0.05 were considered significant. The error bars represent the \pm SEM. The -21 dBm trials showed a reduction in the cells' area compared to the other two trials. All three trials had recorded p-values of <0.01.

The area means of each trial showed a reduction of cell area in the vibrated regions compared to the non-vibrated regions. The greatest reduction of the cell area was displayed in the -21 dBm trials, and the result was expected due to the cells receiving the highest vibrational intensity. The areas of all three non-vibrated regions within each trial did show an increase in cell area compared to the vibrated regions. The -22 dBm trials did not show a great decrease between the two regions, but there was an overall decrease

in area compared to the control plate. The lower area on the non-vibrated portion of the plate was a result of the cells from the vibrate region migrating onto the non-vibrated region. The higher density of cells in the non-vibrated region lowered the amount of area each cell could occupy.

The results characterized the effect of the ultrasound on the cells' adhesion properties to the surface of the plate. In every trial, the areas of the cells were reduced in the vibrated region of the plate compared to the non-vibrated region. The reduction of the cells' area within the vibrated region represents their loss of adhesion strength to the surface.

5.4 Effectiveness of the Ultrasonic Vibrations

From the three trials, ultrasonic vibrations have shown the ability to be used for the control of fibroblast adhesion with results similar to the magnetoelastic materials utilizing mechanical vibrations. The mechanical vibrations revealed a higher cell detachment quantity than the ultrasonic, especially compared with the -25 dBm and -22 dBm of the ultrasound trials. The lower amount of detachment could be attributed to the shorter vibration time of 1 hour compared to the 2 hours vibration in magnetoelastic process. Also, the -21 dBm ultrasonic trial resulted in a high death rate among cells in the targeted area unlike in any of the mechanical trials. Dead cells in the targeted area could cause the problem of an increase in the risk of infection and immune response, as well as damaging of surrounding tissue if the cell death was attributed to cell necrosis. If the ultrasound treatment resulted in the apoptosis process, then there would be no increase in immune response to the area. Previous studies have shown that low intensity ultrasound with a similar intensity to the ones used in this study were shown to result in cell apoptosis [21]. The maximum displacement of the magnetoelastic material, 0.1542 μm , was significantly larger than the three ultrasonic tests with 0.00195 μm , 0.00276 μm , 0.00309 μm , but the dissimilarity was due to the mechanical vibration frequency of 176 kHz compared to the 1 MHz of the ultrasound. The other difference between the two tests was the directions of the vibrations which were shown in Figure 1.6.2. The

vibrations perpendicular to the surface could affect the cells in a different manner than the parallel vibrations by the magnetoelastic materials.

The ultrasonic intensities were used to calculate the applied pressure forces acting upon the fibroblast cells, located in Table 2.1. The applied pressures were found to be 2.9 kPa, 4.0 kPa, and 4.6 kPa for the trials -25 dBm, -22 dBm, and -21 dBm, respectfully, and were calculated using Equation 2.2 and Equation 2.3. The response of the cells to the applied pressures characterizes the relationship of how the amplitude of the mechanical forces is able to manipulate cell behavior.

The detachment of the cells could be attributed to the mechanotransduction qualities of the cells. The cells migrated to a more stable location on the cell plate and away from the direct effect of the ultrasonic waves in the -22 dBm trial. With the information that cells will migrate from an area which does not have static mechanical conditions, implantable devices can utilize these techniques to control the fibrotic response.

5.5 Ultrasound Model for Treatment

The use of ultrasound for the control of the fibrotic response requires the correct ultrasonic intensity to be applied to the cells. The transducer output intensity is determined by the depth of the targeted location and the tissue mediums which will be encountered. The depth of the targeted location influences the ultrasonic wave's power dissipation. Changes in medium densities produce a reflective wave and lower the amount of power transmitted to the target area.

Equation 5.1

$$I_s = \frac{\sigma_{sc}}{4\pi R^2} I_i$$

The ultrasonic wave traveling through a consistent medium experiences a loss in power due to the scattering effect. Any changes within the medium such as density, absorption levels, and compressibility would cause reflective waves to occur and also reduce the intensity at the target location. The amount of power loss due to scattering is

found in Equation 5.1 where (I_s) is the scattering intensity, (I_i) is the incident intensity, (σ_{sc}) is the absorption coefficient of the medium, and (R) is the radius of the ultrasound beam. When using a low intensity ultrasound treatment, the attenuation of the ultrasonic wave is critical to ensure the correct intensity is being applied to the targeted area. The attenuation or gradual loss in intensity, due to scattering and absorption is directly proportional to the frequency and is commonly measured as $\frac{dB}{Hz \cdot cm}$. The incident intensity has to be increased in order to counteract the intensity attenuation within the tissue. Also, tissues with a high density need to be avoided due to their ability to increase the scattering of the ultrasound wave.

$$\text{Equation 5.2} \quad \frac{p_r}{p_i} = \frac{Z_2 \cos \theta_i - Z_1 \cos \theta_t}{Z_2 \cos \theta_i + Z_1 \cos \theta_t}$$

$$\text{Equation 5.3} \quad \frac{p_t}{p_i} = \frac{2Z_2 \cos \theta_i}{Z_2 \cos \theta_i + Z_1 \cos \theta_t}$$

The greatest loss of ultrasound intensity occurs due to reflective waves which arise during changes in medium density as seen in Figure 5.1. The ultrasonic wave passing through different densities of mediums will cause a reflective wave in the relationship in terms of Equation. 5.2, where (Z_1) and (Z_2) are the medium impedances, (θ_i) is the incident angle and, (θ_t) is the transmission angle. The transition to a denser medium than the current medium creates a reflective wave and a reduced transmitted wave. The ultrasonic wave path must be clear of any dense tissues such as bone, which could block the ultrasound transmission. Ultrasound liquid gel or gel pads are used on the transducer-skin contact to facilitate the transmission of ultrasonic waves into the body. Transitions with mediums which are equivalent or similar in densities reduce the amount of reflection while increasing the transmission intensity as seen in Equation 5.3.

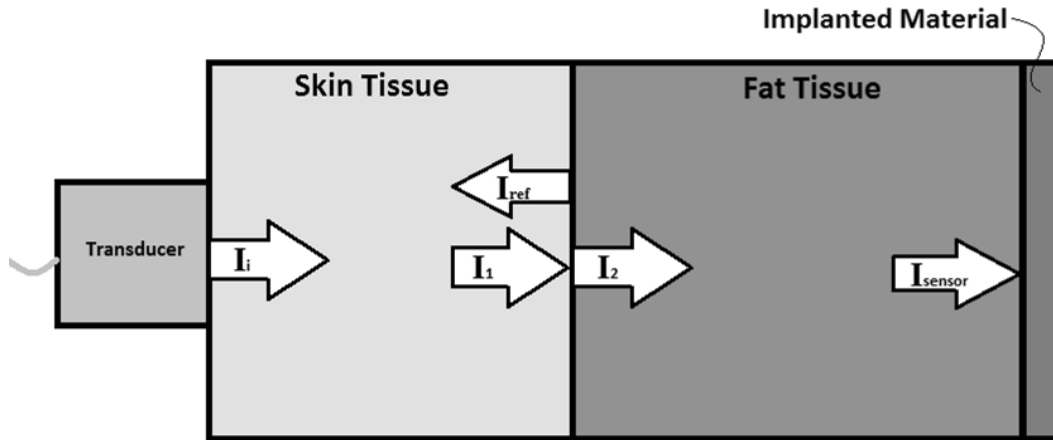


Figure 5.10 –When an incident wave encounters a change in medium, a transmitted wave and reflective wave are developed. The resulting intensity of the transmitted and reflective waves is dependent on the change of medium densities.

The ultrasound treatment utilizes two different effects to the tissues along the target path of the treatment: mechanical and thermal. Mechanical effects are the forces acting on the tissues in the form of pressure forces, compressing and expanding the cells. The thermal effects are caused by the vibrational forces acting on the cells and tissues and increase the temperature of the affected area. The mechanical and thermal effects are both present during all ultrasound treatments, but there are methods for reducing them in order to avoid adverse side effects [23].

5.5.1 Mechanical Effects

The mechanical effects of the ultrasound treatment are due to the compressive waves of the ultrasonic wave as it travels through the mediums. The two major forms of mechanical effects are acoustic cavitations and acoustic streaming. Acoustic cavitations occur when the ultrasonic wave passes through a cavity such as a gas bubble, or air pocket. The cavity expands and compresses in a pulsating manner consistent with the compressive waves of the ultrasound. The vibration of the bubble can cause a buildup of high temperature and pressure if the bubble bursts. The bursting of the cavity also has the possibility of releasing a micro jet of liquid which can damage nearby cells.

Cavitations have a higher probability of occurring in areas such as the intestines and lungs due to the high presence of gas [23, 24].

The mechanical index is used in the determination of whether the mechanical effects are safe for the use or the effects are harmful to the patient. The equation to determine the mechanical index (MI) is shown below:

$$\text{Equation 5.4} \quad MI = \frac{p_{r.3}}{\sqrt{f_c}} \quad [18]$$

The center frequency of the ultrasound signal is represented as f_c and the rarefactional pressure in MPa of the ultrasound field with an attenuation coefficient of 0.3 dB (MHz \cdot cm)⁻¹ is represented by $p_{r.3}$. The value of MI should not be above 1.9 in clinically use ultrasound due to the increased risk of micro bubble cavitations. MI values below 0.2 have shown no effect on the biological system [18].

Acoustic streaming is the formation of a liquid flow around the vibrating bubble within the tissue. Bulk streaming and micro streaming both occur in response to the ultrasonic waves. Bulk streaming has a lessened effect on cells than micro streaming due to being less mechanically powerful. The fluid flow moves in a single direction in line with the ultrasonic beam. Micro streaming is caused due to cavitation effects and propagates from vibrating bubbles. Unlike bulk streaming, micro streaming does not occur in-vivo. Micro streaming is able to cause the cell membrane to become more permeable and stimulates cell activity [23, 24].

5.5.2 Thermal Effects

Thermal effects occur due to the vibrational properties of the ultrasound treatment and cause a rise in temperature which can result in tissue damage. Temperature increases of 1 °C have been shown to have biological effects within the treated tissues [24]. The change in the temperature of the tissue is directly proportional to the intensity of the ultrasonic wave. In order to reduce the thermal effect of the ultrasound, the output intensity can be lowered or the output signal can be pulsed instead of continuous.

Another method to reduce the temperature increase is to constantly move the transducer in the applied area [23, 24]. The tissue's ability to absorb the energy of the ultrasonic wave's intensity directly relates to the tissues thermal heating capacity. The intensity attenuation coefficient (μ) of the medium and distance (x) determine the loss of intensity through the equation:

$$\text{Equation 5.5} \quad I(x) = I_0 e^{-\mu x} \quad [17]$$

The power loss in 5.5.4 is distributed into scattering and absorption losses contributed to the medium with majority being attributed to absorption. The scattering energy is dissipated throughout the tissue while absorption maintains the energy within a localized location. The rate of temperature rise within tissue is characterized by the equation:

$$\text{Equation 5.6} \quad \frac{dT}{dt} = \frac{\mu I}{\rho C} \quad [17]$$

The density of the medium (ρ) and heat capacity (C) has an inverse relationship with the rate of temperature. Tissues with high absorption coefficients such as large proteins and collagen tissues are found to be heated at a higher rate than fat tissue [17].

5.5.3 Ultrasound Treatment Model

The ultrasound treatment has the ability to be used to control fibrosis in a multiple of applications. In order to ensure the correct intensity was applied to the targeted region, calculations were required to determine the losses which would be experienced during the treatment. The intensity losses include reflection, scattering, and absorption. The mediums of the targeted location influenced the amount of loss experienced by the ultrasonic beam. By utilizing the acoustic intensity equations, ultrasound treatment models were designed to ensure the correct ultrasound intensity was applied to the targeted location.

Many implants were surrounded by skin tissue and fat tissue. The thickness of skin tissue varies on the body depending on the location, but on average was 2-3 mm. The depth of the implanted device determines the thickness of the fat tissue, but many devices which were non-surgically implanted were at an approximate depth of 7 mm. In Section 5.5, the -22 dBm trial was determined to create a favorable effect for the control of the fibrotic process and cell adhesion. Assuming the intensity at the targeted site was to be -22 dBm and utilizing the transmission Equations 5.2 and 5.3, as well as the attenuation Equation 5.5, the output intensity of the transducer is found. An assumption is made as the transducer-skin transmission is 100% with the utilization of ultrasound gel. The basis of the assumption was due to the different gel types available, and each gel could differ in medium density.

The two tissues commonly encountered during the ultrasound treatment would be skin and fat tissues. The skin tissue was denser with an acoustic impedance of $1.99 \times 10^6 \frac{kg}{sec \cdot m^2}$ and an attenuation coefficient of $1.57 \frac{dB}{MHz \cdot cm}$ [25], while fat tissues has a impedance of $1.38 \times 10^6 \frac{kg}{sec \cdot m^2}$ and an attenuation coefficient of $0.48 \frac{dB}{MHz \cdot cm}$ [26]. The model was shown in Figure 5.5.1, with the skin and fat tissue mediums.

By utilizing the information above, it was calculated that the required transducer output would be 6.8 dBm in order to achieve the -22 dBm ultrasound intensity at the surface of the implant. An intensity of 6.8 dBm would amount to 4.8 mW. The intensity values throughout the tissue mediums also allow for the analysis of the amount of heat which would be added to the system and could possibly harm the surrounding tissue. Equation 5.6 was used to calculate the heating of the skin and fat tissues throughout the model, and the maximum value was found to be $2.11 \times 10^{-9} \text{ } ^\circ\text{C s}^{-1}$ within the skin tissue. In comparison, common therapeutic transducers with an output of 30 dBm cause a heat increase of $0.048 \text{ } ^\circ\text{C s}^{-1}$ [17]. The low value of the heat increase in relation to time shows that the technique was safe from tissue damage attributed to heat.

6. Conclusion

Fibrosis has the possibility of limiting the functionality and safety of implanted devices such as bone-anchored prosthesis and glucose sensors. The adhesion of fibroblasts has been shown to damage implants and cause harm to the patients. Fibrotic encapsulation of sensors within the body limits the response of the sensor and diminishes their effectiveness. Many implantable devices employ an anti-fouling coating on the surface to resist the attachment of fibroblast, but the coating was not able to maintain the resistance for an extended length of time. The use of therapeutic ultrasound allowed for an in-vitro treatment to enhance the anti-fouling surface of the devices without the devices requiring any modifications. The adhesion of fibroblasts on an implanted surface cannot be halted completely, but through the use ultrasound therapy, it could be controlled.

During the experiments, all three intensities were shown to have an effect on the fibroblast cells' behavior and caused a weakening of their adhesion capabilities. Many of the cells in the -25 dBm (2.9 kPa) trial did not fully detach until an added mechanical force was added from the PBS wash. The cells in the -22 dBm (4.0 kPa) did appear to detach from the targeted area and migrated to a more stable location for reattachment. Finally, the -21 dBm (4.6 kPa) trial caused the highest detachment of cell, but also created the highest death rate of the cell within the targeted area. The dead cell could cause the possibility of an increased immune response which would be detrimental to the function of the implanted device.

The results from the experiment displayed the effectiveness of the therapeutic ultrasound treatment in controlling the fibroblast adhesion. The -22 dBm trial was shown to be most effective out of the three trials. The cells were able to become fully detached without an added mechanical force, and there was no increase in cell deaths.

6.1 Future Work

The experiments were able to display the effectiveness of a therapeutic ultrasound to provide an anti-fouling method on implanted devices. Unfortunately, the experiments were not able to address some of the concerns about the results.

In the -25 dBm trial, the cells were not able to become fully detached from the surface until an added mechanical force was applied. In an *in-vivo* environment, certain devices could experience mechanical forces in the external system from movement, such as a hip joint prosthetic. The added force from the movement in the joint could allow for enough force to detach the cells. The lower intensity of -25 dBm would be beneficial in lowering the heating effect within the tissue.

The rate of movement of the cells in the -22 dBm trial was not able to be characterized. Determination of the response rate in which the cells responded to the ultrasound treatment and initiated their migration would allow for the calculation of the treatment duration. Also, the direction of cell relocation was determined to follow the concentration gradient which could help predict the direction of the cells' movement within the body and across the surface of the implant. Further testing should be done on the cells in a 3-dimensional environment to aid in the prediction of the cell migration.

Theoretical calculations were completed of the ultrasound's thermal and mechanical effects within the biological system, but more sophisticated models would be required to accurately portray the effects.

References

1. Rolfe, B., et al., *The Fibrotic Response to Implanted Biomaterials: Implications for Tissue Engineering*, in *Regenerative Medicine and Tissue Engineering - Cells and Biomaterials*, P.D. Eberli, Editor. 2011. p. 551-568.
2. Vlaisavljevich, E., et al., *Magnetoelastic Materials as Novel Bioactive Coating for the Control of Cell Adhesion*. IEEE, 2011. **58**(3): p. 698-704.
3. Anderson, J.M., *Biological responses to materials*. Annu. Rev. Mater. Res., 2001. **31**: p. 81-110.
4. Gerritsen, M., *Problems Associated with Subcutaneously Implanted Glucose Sensors*. Diabetes Care, 2000. **23**(2): p. 143.
5. Moussy, F., *Implantable Glucose Sensor: Progress and Problems*. IEEE, 2002. **1**: p. 270-273.
6. Wisniewski, N. and M. Reichert, *Methods for reducing biosensor membrane biofouling*. Colloids and Surfaces B: Biointerfaces, 2000. **18**: p. 197-219.
7. Yu, Q., et al., *Anti-fouling bioactive surfaces*. Acta Biomaterialia, 2011. **7**(4): p. 1550-1557.
8. Sharma, S., R.W. Johnson, and T.A. Desai, *XPS and AFM analysis of antifouling PEG interfaces for microfabricated silicon biosensors*. Biosensors and Bioelectronics, 2004(20): p. 227-239.
9. Ziegler-Graham, K., et al., *Estimating the Prevalence of Limb Loss in the United States: 2005 to 2050*. Arch Phys Med Rehabil, 2008. **89**: p. 422-429.
10. Dungal, P., et al., *Study of the effects of tissue reactions on the function of implanted glucose sensors*. Biomedical Materials Research Part A, 2007: p. 699-106.
11. Boyle, J.P., et al., *Projection of the year 2050 burden of diabetes in the US adult population: dynamic modeling of incidence, mortality, and prediabetes prevalence*. Population Health Metrics, 2010. **8**(29).
12. Centers for Disease Control and Prevention, *National diabetes statistics report: estimates of diabetes and its burden in the United States, 2014*, US Department of Health and Human Services, Editor. 2014: Atlanta, GA.
13. Koschwanetz, H.E. and W.M. Reichert, *In Vitro, In Vivo and Post Explantation Testing of Glucose-Detecting Biosensors: Current Methods and Recommendations*. Biomaterials, 2007. **28**(25): p. 3687-3703.
14. Brosig, M., *Mechanotransduction in Fibroblasts*, in *Fredrich Miescher Institute for Biomedical Research*. 2011, University of Basel: Munich. p. 1-89.
15. Solovchuk, M.A., et al., *Effect of acoustic streaming on tissue heating due to high-intensity focus ultrasound*. arXiv, 2011. **1111.2908**.
16. Speed, C.A., *Therapeutic ultrasound in soft tissue lesions*. Rheumatology, 2001. **40**: p. 1331-1336.
17. Haar, G.t., *Review Therapeutic Ultrasound*. Journal of Ultrasound, 1999(9): p. 3-9.
18. Chen, Z., *Assessment of ultrasound field properties and the potential effect on cells*, in *Medical Engineering*. 2013, Royal Institute of Technology: Stockholm.
19. Doan, N., et al., *In Vitro Effects of Therapeutic Ultrasound on Cell Proliferation, Protein Synthesis, and Cytokine Production by Human Fibroblasts, Osteoblast, and Monocytes*. Journal of Oral and Maxillofacial Surgery, 1999. **57**: p. 409-419.

20. Rasband, W.S. *ImageJ*. 1997-2014; Available from: <http://imagej.nih.gov/ij/>.
21. Taylor, R.C., S.P. Cullen, and S.J. Martin, *Apoptosis: controlled demolition at the cellular level*. *Nature: Molecular Cell Biology*, 2008. **9**: p. 231-241.
22. Feng, Y., Z. Tian, and M. Wan, *Bioeffects of Low-Intensity Ultrasound In Vitro: Apoptosis, Protein Alteration, and Potential Molecular Mechanism*. *Journal of Ultrasound Medicine*, 2010(29): p. 963-974.
23. Baker, K.G., V.J. Robertson, and F.A. Duck, *A Review of Therapeutic Ultrasound: Biophysical Effects*. *Physical Therapy*, 2001(81): p. 1351 - 1358.
24. Nyborg, W.L., P.L. Carson, and E.L. Carstensen, *Diagnostic Ultrasound Safety, in Exposure criteria for medical diagnostic ultrasound. II. Criteria based on all known mechanisms. .* 2002, National Council on Radiation Protection and Measurements: Bethesda, Md.
25. Azhari, H., *Typical Acoustic Properties of Tissues*, in *Basics of Biomedical Ultrasound for Engineers*. 2010, John Wiley & Sons, Inc.
26. Culjat, M.O., et al., *A review of tissue substitutes for ultrasound imaging*. *Ultrasound in Medicine and Biology*, 2010. **36**(6): p. 861-873.